

# Developing Photocathode Materials for p-type Dye-Sensitized Solar cells

Elisabetta Benazzi<sup>a</sup>, John Mallows<sup>a</sup>, Gareth H. Summers<sup>a</sup>, Fiona A. Black<sup>a</sup>, and Elizabeth A. Gibson<sup>\*a</sup>

<sup>a</sup>Energy Materials Laboratory, Chemistry, School of Natural and Environmental Science, Newcastle University, Newcastle upon Tyne, NE1 7RU, UK. E-mail: Elizabeth.gibson@ncl.ac.uk

**Dye-sensitized solar cells are photoelectrochemical devices, which are of great interest due to their ease of fabrication and attractive design. This review details the progress made over the last 20 years into the development of more efficient p-type DSCs with the goal of combining both p and the more widely studied n-type (TiO<sub>2</sub>)-based photoelectrodes in tandem-DSCs. Such tandem architectures offer an opportunity to collect more light, more efficiently by overcoming the thermodynamic limits of single-junction devices. The main components of the p-DSCs, such as the variety of different sensitizers, p-type semiconductors and electrolytes are introduced and their typical performance in devices are compared. The kinetics of light-induced charge transfer at the interfaces between these materials are also discussed and suggestions are made as to which factors could be a priority for future research to increase the performance of p-type DSC to match state-of-the-art TiO<sub>2</sub>-based devices, which is necessary for a step change in the conversion efficiency.**

## Introduction

Energy is crucial for sustaining human life on Earth and has always underpinned technological development. Since the industrial revolution, the use of fossil fuels over the past two and a half centuries has facilitated technological innovations and improved living standards for a large part of the global population. Nowadays, the global energy consumption is approximately 18 TW per year.<sup>1</sup> Consumption is predicted to rise to 27.6 TW by 2050 and 43.0 TW by 2100.<sup>2</sup> Currently, most of this energy demand is fulfilled by finite and environmentally damaging fossil fuels; policies have been set to reduce greenhouse gas emissions by the development of the renewable energy sector.<sup>3,4</sup> 120 000 TW of solar energy from sunlight strikes the earth, making it the most abundant renewable energy source. Despite this abundance and the increased efficiency of commercial solar cells, solar technology provides less than 0.5% of global primary energy demand and contributes less than 1% toward the production of electricity (which has a 22% contribution from renewable sources).<sup>1,5,6</sup> Technologies for directly harnessing solar energy include photovoltaics (PV), solar thermal and solar fuel (photoelectrochemical/photobiological cells). Single-junction silicon, a 1<sup>st</sup> generation PV technology, dominates the market as the most utilised technology integrated into infrastructure. Light absorption and charge separation occur in the same material by means of an internal electric field (a p-n junction).<sup>3,7</sup> Silicon has an indirect band gap, so a thick layer of high purity and crystalline absorber material is required, which is associated with energy intensive and expensive manufacturing processes. Additionally, the performance of this technology is limited by the Shockley-Queisser (SQ) limit, a thermodynamic limit applicable to single-junction devices. The maximum solar conversion efficiency of PV is approximately 33%, for an optimum bandgap of 1.34 eV and using an AM 1.5 solar spectrum.<sup>8</sup> Such limitations have stunted the overall

applicability of these devices. Emerging PV technologies, including tandem and multi-junction devices have the potential to overcome the SQ limit.

Emerging technologies based on nanotechnology are of particular interest because they offer alternative applications to c-Si, in part due to different processing methods and operational mechanisms. Dye-sensitized solar cells (DSCs), in particular, differ from Si-PVs in that the functions of light absorption and charge separation are separated and carried out by different components. Theoretically, this allows cheaper, lower purity materials to be used, as defects are not such a prominent issue. The advantages of DSCs include using abundant materials, a simple manufacturing process and a wide choice of usable substrates. These devices are based on nanocrystalline TiO<sub>2</sub> and a consequence of this is that the angle of incident light is not critical and they have been shown to work under low-light conditions.<sup>9,10</sup> This means they have the potential for integration into windows or building materials and for use in indoor applications. Furthermore, tandem DSC devices (p-n DSCs) can surpass the SQ limit (theoretically  $\geq 43\%$ ) by increasing the spectral response of the device without sacrificing photovoltage.<sup>11,12</sup>

## Discussion

### 1. p-DSCs

The first p-DSC was reported in 1999 by Lindquist and co-workers.<sup>13</sup> The cell was made using the same components as for an n-DSC (Figure 1), but the TiO<sub>2</sub> semiconductor was replaced with a layer of NiO; a p-type semiconductor. An overall PCE of 0.0076% was obtained using erythrosin B as a sensitizer. Indeed, p-type devices operate in a similar fashion to n-DSCs, however, as the majority charge carriers in NiO are positive holes (h<sup>+</sup>), the electron flow occurs in the reverse direction. In an n-type device, electron transfer occurs from the excited dye into the conduction band of TiO<sub>2</sub>. Conversely, for a p-type device

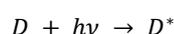
electron transfer occurs from the valence band of the semiconductor to the excited dye. A schematic representation of a NiO-based p-DSC is provided in Figure 1 and the individual

**Figure 1.** *Top:* Schematic representation of the charge transfer processes occurring within a TiO<sub>2</sub>-based n-DSC. *Bottom:* Schematic representation of the charge transfer processes occurring within a NiO-based p-DSC.

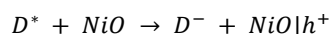
components are discussed in more detail in the following paragraphs.

The charge transfer processes that occur in a p-DSC under operation are summarised in Figure 1. These are as follows:

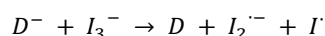
Photoexcitation of the dye (D) via the absorption of a photon to form an electronic excited state (D\*):



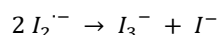
Electron transfer from the valence band of NiO to the excited dye (or hole transfer from the dye to NiO):



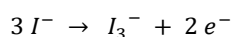
Regeneration of the ground state of the dye by the oxidised species in the electrolyte, which involve radical species:



The reduced dye is first regenerated by triiodide to form the diiodide radical.<sup>14</sup> This undergoes disproportionation to form triiodide and iodide:



Regeneration of the reduced species in the electrolyte occurs at the counter electrode:

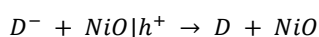


These forward charge transfer processes are in competition with several recombination pathways:

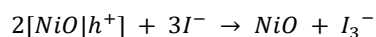
Excited state decay of the dye (radiative and non-radiative):



Recombination between the reduced dye and a hole in NiO:



Recombination of a hole in NiO with the reduced species in the electrolyte:



Over the past 20 years, considerable effort has been made to improve the device performance by reducing recombination and enhancing charge transfer, including the design of novel sensitizers with long-lived charge separated states, the design of custom-made electrolytes and a search for new semiconductors as alternatives to the well-established, but problematic NiO. In the following paragraphs we will go through each p-type DSC component to provide insight into progress that has been made and opportunities for future research.

## 2. Sensitizers

The requirements of an ideal dye include the capability of absorbing photons in the visible-NIR region, a broad absorption profile and high extinction coefficient; an anchoring unit which ensures absorption on the SC surface (typically carboxylic acids, phosphonates and pyridine anchoring units), suitably positioned HOMO and LUMO levels to promote efficient charge transfer and dye regeneration (the HOMO needs to be more positive than the valence band edge ( $V_{BE}$ ) of the semiconductor and the LUMO needs to be more negative than the redox potential of the electrolyte).<sup>15-19</sup> Furthermore, the dye structure should promote a long-lived charge-separated state. This is usually attempted by following a donor-acceptor 'push-pull' design, where electron density will be shuttled to the periphery of the dye following charge transfer from the semiconductor. Many research groups are working on designing new sensitizers to improve the efficiency of p-DSCs, which has produced a wide range of publications.<sup>20-22</sup> Figure 2 provides a comparison of the DSC performances of around ninety dyes that have been designed for p-DSCs. Ruthenium refers to ruthenium complexes used as dyes and double acceptor/anchor refers to triphenylamine based push-pull dyes, with either one or two acceptor groups, depending on the configuration chosen (Figure 3).  $J_{SC}$  and  $V_{OC}$  refer to the short-circuit photocurrent density and open-circuit voltage respectively.

**Figure 2.** A comparison of p-DSC performances for various reported dyes tested with an  $I^-/I_3^-$  electrolyte.

**Figure 3.** Schematic representation of triphenylamine 'push-pull' dyes bearing one or two acceptor groups. L = linker group and A = acceptor unit.

### 2.1 Metal complexes based dyes

In general, dyes based on ruthenium complexes perform worse than organic dyes, which is the opposite trend to the majority of n-DSCs. Indeed, in n-DSCs, ruthenium complexes are efficient sensitizers that outperformed organic dyes for a long time. In contrast, in p-type systems, the benchmark N719 dye was the

**Figure 4.** Molecular structure of ruthenium dyes used for NiO-based p-DSCs.<sup>26-32</sup>

first ruthenium photosensitizer tested with NiO.<sup>23</sup> A 'desensitizing' effect was seen for NiO/N719, where the dyed

devices performed worse than NiO alone ( $J_{SC} = 8$  vs.  $46 \mu\text{A cm}^{-2}$  for NiO/N719 and NiO respectively). The authors postulated that N719 was forming a dye-iodide complex, as has been reported previously for n-DSCs, which can catalyse the oxidation of iodide.<sup>24</sup> This could lead to enhanced electrolyte/NiO recombination in a p-type device. The fully protonated analogue N3 was also tested in p-DSCs, reporting a negligible  $J_{SC}$  and no photocurrent response at monochromatic wavelengths that could be attributed to the dye.<sup>25</sup> These dyes were thought to perform poorly as they were engineered to have higher electron densities at the semiconductor surface following excitation. This would promote electron transfer into the TiO<sub>2</sub> conduction band in an n-type device, but has the opposite effect of inhibiting NiO-dye electron transfer (and promoting dye/NiO recombination) in a p-type device. While N719 and N3 did not prove suitable for use in a p-DSC, other ruthenium dyes have proved more successful by adopting a donor-acceptor design. Figure 4 shows a selection of ruthenium dyes that have been used to produce photocurrent densities  $> 2 \text{ mA cm}^{-2}$  when utilised in a p-DSC in conjunction with NiO. Most of these (the OX series, K1 and SL1) were designed with a triphenylamine donor, so that following excitation, electron density would be located on the ruthenium core, away from the semiconductor surface. This design, which was intended to inhibit charge recombination between the reduced dye molecules and holes in NiO, was successful in producing higher photocurrent densities. The dyes that produced a  $J_{SC}$  close to or higher than  $3 \text{ mA cm}^{-2}$  were K1, O3, O18 and [Ru(bpy)<sub>2</sub>(H<sub>5</sub>)] ( $J_{SC} = 2.91, 3.04, 3.43$  and  $4.06 \text{ mA cm}^{-2}$  respectively).<sup>26-29</sup> Interestingly, the highest performance (PCE = 0.139%) was obtained using the structurally simplest dye, [Ru(bpy)<sub>2</sub>(H<sub>5</sub>)]. A structural analogue (O11) has been previously reported for use in p-DSCs, which instead contained a carboxylic acid anchoring unit.<sup>30</sup> With the carboxylic acid anchoring group, much lower device efficiencies were obtained ( $J_{SC} = 1.16$  and PCE = 0.033% O11 vs.  $J_{SC} = 4.06 \text{ mA cm}^{-2}$  and PCE = 0.139% for [Ru(bpy)<sub>2</sub>(H<sub>5</sub>)]), despite the apparent subtle structural difference. [Ru(bpy)<sub>2</sub>(H<sub>5</sub>)] was isolated as a zwitterion, so it is possible that the reduced electron density on ruthenium imparts some charge transfer character.<sup>29</sup> This could increase photocurrent density by reducing recombination. A similar effect was reported for the ruthenium dyes with a carboxylic acid anchoring group by inserting additional phenyl groups between bipyridine and benzoic acid, thereby increasing the spatial separation between NiO and the ruthenium core. Interestingly, novel push-pull ruthenium diacetylide complexes (SL1 and SL2,  $\epsilon > 2 \times 10^4 \text{ M}^{-1} \text{ cm}^{-1}$ ) have also been investigated by Odobel and co-workers, with SL1 showing superior performance ( $J_{SC} = 2.25 \text{ mA cm}^{-2}$ ,  $V_{OC} = 104 \text{ mV}$ ,  $ff = 34\%$ , PCE = 0.079%) which is attributed to an increased dye loading over SL2.<sup>31</sup> Notably, both complexes had a modest driving force for hole injection (0.25 - 0.3 eV), but with alternative push-pull units a highly efficient push-pull ruthenium complex could be realised. Compared to n-type systems, where the anchoring of the sensitizer to the TiO<sub>2</sub> surface has been thoroughly studied, rather less is understood regarding the best binding groups for

NiO.<sup>32</sup> Besides well-known ruthenium complexes with carboxylic and phosphonic acids as anchoring groups, Odobel and co-workers investigated four ruthenium complexes with different anchoring groups, either carboxylic acid, biscarbodithioic acid, catechol and methyl phosphonic acid.<sup>15</sup> Their experiments demonstrated that both catechol and methyl phosphonic acid are promising alternative binding groups for NiO sensitizers. Methyl phosphonic acid is a valuable anchoring group which has been shown to form a stable linkage with a metal oxide surface, such as TiO<sub>2</sub>. Catechol potentially enhances the electronic coupling with the semiconductor (the HOMO of the sensitizer mixes with the wave function of the valence band of NiO) because it is more electron rich than the conventional carboxylic acid.

**Figure 5.** Structures of the iridium complexes IrPhen, IrDPQCN2, IrBpystyryl.<sup>33</sup>

Additionally, other transition metal complexes, based on iridium have been investigated for application in p-DSCs. Iridium complexes are of particular interest due to the strong oxidizing power of their excited state, favouring hole injection into the VB of the SC. Three novel cyclometalated iridium complexes (IrPhen, IrDPQCN2, IrBpystyryl) (Figure 5) were reported by Odobel and co-workers.<sup>33</sup> IrDPQCN2 showed the best performance ( $\text{Co}^{\text{II/III}}$ :  $J_{SC} = 0.25 \text{ mA cm}^{-2}$ ,  $V_{OC} = 508 \text{ mV}$ ,  $FF = 54\%$ , PCE = 0.068%), which was attributed to a longer-lived triplet excited state with respect to the other complexes. It is worth mentioning that generally the  $J_{SC}$  was relatively low due to the low light harvesting efficiency over the visible spectrum of these iridium complexes.

**Figure 6.** Iridium biscyclometalated complexes prepared (AS9-15). Ancillary ligands used for p-type complexes synthesis (N<sup>\*</sup>N): (AS9) bipyridine; (AS10) phenanthroline; (AS11) dipyrrodo[3,2-a:20-30-c]-phenazine; (AS12) 4-nitrobipyridine; (AS13) 4,4'-dinitrobipyridine; (AS14) N,N'-bis(4-methoxyphenylimino)acenaphthene; (AS15) N,N'-bis(phenylimino)acenaphthene.<sup>34</sup>

Furthermore, Elliott and co-workers synthesised seven iridium complexes (Figure 6), comprising of two 4-(pyrid-2-yl) benzoic acid anchoring ligands and alternate diamine electron accepting ancillary ligands.<sup>34</sup> The design of the p-type dyes reported in Figure 6 comes mainly from the need to prevent the recombination of the injected hole with the excited electron together with a reasonable absorption coefficient for visible light. The carboxylate anchoring groups were placed on the electron donating anionic aryl groups. This should maintain efficient anchoring onto the electrode but ensure localization of the HOMO on these moieties. Use of a neutral electron accepting ancillary ligand trans to the anchoring arylcarboxylate rings thus ensures localization of the LUMO away from the anchoring groups, thereby maximising charge separation and minimising recombination. AS14 showed the best device performance ( $I_3/I_1$ :  $J_{SC} = 1.12 \text{ mA cm}^{-2}$ ,  $V_{OC} = 0.10$ ,  $FF = 36.8\%$ , PCE = 0.043%), displaying encouraging results for a new generation of iridium-based p-type dyes.

**Figure 7.** [Ir(C<sup>^</sup>N<sup>^</sup>C)(N<sup>^</sup>N)Cl] [where C<sup>^</sup>N<sup>^</sup>C = 2-(bis(4-(tert-butyl)phenyl)methyl)pyridinato and N<sup>^</sup>N is diethyl [2,20 -bipyridine-4,40 -dicarboxylate].<sup>35</sup>

Zysman-Colman *et al.* recently reported an Iridium complex (Figure 7), bearing an unusual tripodal tridentate C<sup>^</sup>N<sup>^</sup>C ligand forming three six membered rings around the iridium centre.<sup>35</sup> Despite the interesting structure, DSCs using the dye achieved only an average PCE of 0.49%, comparable to other Ir(III) dyes. This was attributed to the modest absorption coefficient which leads to weak light harvesting in the visible region and low short-circuit current. The design of an alternative anchoring group could open the way to higher performing DSCs in the future.

## 2.2 Organic push-pull dyes

**Figure 8.** Molecular structures of commercial dyes, coumarin C343 and erythrosin B.<sup>13,36</sup>

**Figure 9.** Molecular structure of PMI-acceptor dyads tested for p-DSCs.<sup>37-39</sup>

In contrast to organometallic dyes, more satisfying results have been obtained with organic dyes. In early publications on NiO-based p-DSCs, commercial dyes such as coumarin 343 (C343) and erythrosin B were used as the sensitizer (Figure 8).<sup>36</sup> These served as proof-of-concept reports for dye-sensitized NiO as a photocathode, however the devices were limited by low efficiencies which was attributed to fast recombination between the reduced dye molecules and holes in NiO.<sup>36,37</sup> Slowing down this recombination process is crucial to improve the performances of p-DSCs. Morandeira and co-workers reported the first dye designed specifically for use in p-DSCs (PMI-NDI) as shown in Figure 9.<sup>37</sup> In this perylene system, a long-lived charge separated state was formed in the presence of the naphthalene diimide (NDI) acceptor. The dyad achieved a quantum efficiency three times greater than the analogous dye without NDI. A variety of perylene based donor-acceptor dyads were tested with varying acceptor units (NDI or C<sub>60</sub>, Figure 9) and in each case higher performances were obtained with an acceptor group present.<sup>39</sup> In a later publication, a p-DSC constructed using PMI-NDI sensitized NiO and a Co<sup>II/III</sup>-based redox electrolyte obtained an overall PCE of 0.20%, in part due to a greatly increased V<sub>OC</sub> of 350 mV.<sup>39</sup> This work highlighted the necessity of designing donor-acceptor dyes specifically engineered for NiO-based p-DSCs to increase device efficiencies (Figure 10).

**Figure 10.** Schematic representation of the 'push-pull' design used for p-DSCs.

**Figure 11.** Molecular structure of the triphenylamine push-pull dye P1.<sup>40,41</sup>

One of the first push-pull dyes to achieve a higher J<sub>SC</sub> was the triphenylamine-based dye P1 (Figure 11) and the design has heavily influenced the development of many subsequent dyes for p-DSCs.<sup>40</sup> This dye combined a triphenylamine donor unit and two dicyanovinylene acceptors, linked using thiophene bridges, with a carboxylic acid anchoring group. In the initial publication, P1/NiO p-DSCs produced a J<sub>SC</sub> of 1.52 mA cm<sup>-2</sup> and an IPCE of 18%, with an overall PCE of 0.05%.<sup>25</sup> Devices made using P1 were later optimised, giving IPCEs of 35% and then 63%, with an optimised PCE of 0.15%.<sup>39,42</sup> It remains a benchmark dye when optimising new systems (see below). Another highly efficient set of dyes (published almost at the same time) is the PMI-nT-TPA series (Figure 12).<sup>42</sup> Here, a perylenemonoimide (PMI) acceptor is coupled to a triphenylamine donor by an oligothiophene spacer of varying length. The dyes are adsorbed onto NiO through two carboxylic acid groups on the triphenylamine donor. Increasing the oligothiophene length produced longer-lived charge separated states (see section 3), which greatly increased device performances (PCE = 0.09%, 0.19% and 0.41% for n = 1, 2 and 3 respectively). While the J<sub>SC</sub> for PMI-6T-TPA and P1 were similar (J<sub>SC</sub> = 5.35 vs. 5.48 mA cm<sup>-2</sup>), the PCE was found to be over twice as high, at the time, for PMI-6T-TPA due to the larger V<sub>OC</sub> (218 mV vs. 84 mV).<sup>43</sup> The higher V<sub>OC</sub> could be attributed to reduced electrolyte/NiO recombination, due to the presence of long sterically hindering alkyl chains. Alternatively, it could be due to differences in NiO preparation, as NiO films sensitized with PMI-6T-TPA were constructed using a screen-printing paste prepared from NiO nanoparticles, instead of the sol-gel route used for P1. The PCE of p-DSCs constructed utilising PMI-6T-TPA increased from ca. 0.60% with I<sup>-</sup>/I<sub>3</sub><sup>-</sup> redox couple to 1.20% and 2.51% using electrolytes based on Co(en)<sub>3</sub> and Fe(acac)<sub>3</sub> respectively (see section 4).<sup>44,45</sup> The latter remains the record PCE for a NiO-based p-DSC.

**Figure 12.** Molecular structure of the triphenylamine-peryene dyes PMI-nT-TPA.<sup>42,44,45</sup>

The success of P1 and PMI-6T-TPA sparked renewed interest into designing triphenylamine-based donor-acceptor dyes. Since these reports, the majority of dyes for p-DSCs contain either diphenylamine or triphenylamine donor groups. Triphenylamine has likely seen such widespread attention due to its strong electron-donating ability, ease of functionalisation and non-planar shape which can help reduce aggregation. Due to these reasons, hundreds of arylamine-containing molecules have been designed for DSCs and organic solar cells.<sup>46,47</sup> Most new dye designs aim to modify the acceptor or linker groups.<sup>48-51</sup> There are only a few reports of modified anchoring structure, such as a recent paper by Fielden *et al.* on which a series of dyes with a pyridyl anchoring group was reported (Figure 13).<sup>15,17,71</sup>

**Figure 13.** Chemical structures of the dyes 1 to 6 reported by Fielden *et al.*<sup>71</sup>

Additionally, dyes with two acceptor groups tend to produce a higher J<sub>SC</sub>. As shown in Figure 3, 65% of reported dyes with the

double acceptor structure produced a  $J_{SC} \geq 3 \text{ mA cm}^{-2}$ , compared to 26% for dyes with the double anchor structure. The structures of some of the dyes which generated the highest reported  $J_{SC}$  are provided in Figure 14 and Figure 15. The highest  $J_{SC}$  reported for a p-DSC was produced using CAD3 ( $J_{SC} = 8.21 \text{ mA cm}^{-2}$ ).<sup>48</sup> This was based on the P1 design but had two cationic indolium groups as electron acceptors. This high performance was attributed to the strong absorption properties of the dye ( $\lambda_{max} = 614 \text{ nm}$ ,  $\epsilon = 95,000 \text{ dm}^3 \text{ mol}^{-1} \text{ cm}^{-1}$ ) compared to related dyes with only one indolium acceptor (CAD1 and CAD2).<sup>52</sup>

**Figure 14.** Molecular structure of highly performing push-pull dyes with the double acceptor design; CAD1, CAD2, CAD3<sup>48,52</sup>

**Figure 15.** Molecular structure of highly performing push-pull dyes with the double acceptor design; T3H and T4H.<sup>55</sup>

Yang and co-workers studied the effect of increasing the donor-anchor separation of the P1 structure, by varying the oligothiophene length from four to six units (Figure 15).<sup>53-55</sup> The highest performance was achieved with four thiophenes (T3H). They found that, despite the increased conjugation length and stronger absorbance with five and six thiophenes, after four units the photocurrent decreased due to unfavourable charge transfer from NiO to the dye. Finally, using four thiophenes units as the optimum separation length, the dicyanovinylene acceptor groups were substituted for 1,3-diethyl-2-thiobarbituric acid (T4H).<sup>55</sup> A broader absorption profile was obtained that stretched further into the near infrared (NIR), which resulted in a higher light harvesting ability of the device. Consequently, the device sensitized with T4H produced a higher  $J_{SC}$  than the one which utilised T3H ( $J_{SC} = 5.57$  and  $6.74 \text{ mA cm}^{-2}$  for T3H and T4H respectively). A higher  $V_{OC}$  of 152 mV, compared to 101 mV for CAD3, meant that T4H produced a higher overall PCE (PCE = 0.32% for T4H and 0.25% for CAD3).

**Figure 16.** Molecular structure of the BH dye series.<sup>56</sup>

Another series of particular interest is the BH series (Figure 16), which was designed based on PMI-6T-TPA, with two oligothiophene-PMI acceptor groups and one carboxylic acid anchor.<sup>56</sup> The presence of an additional acceptor increased the molar extinction coefficient due to the extended conjugation ( $\epsilon = 84,000 - 96,000 \text{ dm}^3 \text{ mol}^{-1} \text{ cm}^{-1}$  for the BH series vs  $67,000 \text{ dm}^3 \text{ mol}^{-1} \text{ cm}^{-1}$  for PMI-6T-TPA). The highest p-DSC performances were obtained with BH4, as although extinction coefficients increased with increasing oligothiophene length, the dye loading decreased. BH6 had a dye loading three times lower than BH4, which decreased the  $J_{SC}$ . This is a different trend with respect to the PMI-nT-TPA dyes, in which the  $J_{SC}$  and overall PCE increased with increasing conjugation length. Dye loading for the PMI-nT-TPA series was not studied, but it is possible that the two anchoring groups induced a more ordered dye orientation on the NiO surface. Therefore, increasing the

thiophene length would not significantly increase the overall 'footprint' of the dye. Whereas for the BH series, the long thiophene chains are orientated more horizontally and so increasing their length could reduce dye loading. Devices made with BH4 produced higher photocurrents than both PMI-4T-TPA and PMI-6T-TPA. The overall performance of BH4 was higher than PMI-4T-TPA, but lower than PMI-6T-TPA, due to a reduced  $V_{OC}$  (BH4;  $J_{SC} = 7.40 \text{ mA cm}^{-2}$ ,  $V_{OC} = 128 \text{ mV}$ , FF = 0.30, PCE = 0.28%, PMI-4T-TPA;  $J_{SC} = 3.40 \text{ mA cm}^{-2}$ ,  $V_{OC} = 176 \text{ mV}$ , FF = 0.32, PCE = 0.19%, PMI-6T-NDI;  $J_{SC} = 6.26 \text{ mA cm}^{-2}$ ,  $V_{OC} = 243 \text{ mV}$ , FF = 0.39, PCE = 0.60%). While significant improvements were obtained for devices made using PMI-6T-TPA in conjunction with transition metal-based electrolytes, the BH series was only tested with  $I^-/I_3^-$  (see section 4).

Excluding the PMI-nT-TPA series, many dyes that adopt the double anchor design do not produce a high  $J_{SC}$ . However, a series of fluorene-bridged biphenylamine-perylenemonoimide dyes have been recently successfully studied (Figure 17). In the zzx-op series, the fluorene bridge is directly appended to biphenylamine, which will improve donor/acceptor coupling. In the first publication by He *et al.* the linker groups were varied between fluorene (zzx-op1), fluorene-3,4-ethylenedioxythiophene (EDOT, zzx-op2) and fluorene-EDOT-thiophene (zzx-op3).<sup>51</sup> There was a broader spectral coverage as the conjugation length increased, which was expected to increase the  $J_{SC}$ . However, the  $J_{SC}$  decreased in the order of  $4.36 > 4.00 > 3.80 \text{ mA cm}^{-2}$  (respectively) as the spacer length increased. The  $V_{OC}$  and fill factors of the devices were mostly unaffected ( $V_{OC}$  and FF ranged from 109-112 mV and 0.36-0.38 respectively), therefore the PCE decreased with the same trend for zzx-op1, zzx-op2 and zzx-op3 of 0.18% > 0.16% > 0.15%, respectively. These differences could not be rationalised on the basis of absorption properties or dye loading, as all three dyes had a similar loading of  $2.09 - 2.15 \times 10^{-7} \text{ mol cm}^{-2}$ . The differences were therefore attributed to a decreasing driving force for charge transfer. As the conjugation length increased, the HOMO became more negative which decreased the driving force. Injection quantum yields of 90% > 54% > 39% were calculated for zzx-op1, zzx-op2 and zzx-op3, respectively. Based on these measurements it was proposed that a driving force of  $\approx 0.80 \text{ eV}$  is necessary for high charge transfer quantum yields.

**Figure 17.** Molecular structure of the zzx-op series, a set of highly performing fluorene based push-pull dyes with the double anchor design.<sup>50,51</sup>

As fluorene proved to be the optimum linker unit, in a subsequent publication the team looked at extending the fluorene length (zzx-op1-2 and zzx-op1-3).<sup>50</sup> As the conjugation length was increased the driving force for charge transfer remained mostly unaffected but charge recombination to NiO was reduced. The highest efficiency was obtained with two fluorene spacers (zzx-op1-2,  $J_{SC} = 7.57 \text{ mA cm}^{-2}$ ,  $V_{OC} = 117 \text{ mV}$ , FF = 0.40, PCE = 0.353%). This was attributed to a trade-off between increased donor/acceptor separation and the flexibility of the fluorene chain. As the fluorene bridge became longer, the increased spatial separation between the donor and

acceptor groups would likely hinder recombination between the reduced dye and NiO. Conversely, with shorter chains the dyes could form a more compact layer, which could inhibit recombination between the electrolyte and NiO. zxx-op1-2 was argued to have the correct chain length to balance these two factors, leading to the highest performances. Despite their similarities to the PMI-nT-TPA dyes, none of the zxx-op series were tested with transition metal-based electrolytes.

**Figure 18.** Molecular structures of the p-type dye molecules W1, W2, and W3.<sup>57</sup>

A series of double anchor novel D-A-A (donor-acceptor-acceptor) based sensitizers (W1, W2 and W3) were reported by Zhu and co-workers (Figure 18).<sup>57</sup> In this series an electron withdrawing 2,1,3-benzothiadiazole (BT) moiety was introduced as a  $\pi$ -bridge connecting a triphenylamine donor and alternative acceptor moieties. All dyes exhibited a PCE exceeding 0.1%, with W2 a sensitizer containing an octyl 2-cyanoacrylate acceptor showing the superior performance ( $J_{SC} = 4.16 \text{ mA cm}^{-2}$ ,  $V_{OC} = 121 \text{ mV}$ ,  $FF = 0.33$ ,  $PCE = 0.166\%$ ). The higher light-harvesting efficiency leads to a higher photocurrent in W2. In addition, electrochemical impedance spectroscopy (see section 3) (EIS) studies suggest slower charge recombination at the metal oxide/electrolyte interface and a faster hole transporting ability of W2. This encouraging result indicates the potential of such D-A-A systems for the creation of high-performance photosensitizers for p-type photocathodes.

All these dye series exemplify the double anchor design. On the other hand, a recently reported push-pull thienoquinoidal dye is the antithesis to this design, with a small conjugation length and little donor/acceptor separation (QT-1, Figure 19). Despite this, the dye produced one of the highest reported  $J_{SC}$  values of  $8.20 \text{ mA cm}^{-2}$ . Coupled with a  $V_{OC}$  of 120 mV and an FF of 0.34, this dye had an overall PCE of 0.33% when tested with the  $I^-/I_3^-$  electrolyte. It also proved to be successful when used with a  $Co^{II}/Co^{III}$ -based electrolyte ( $J_{SC} = 6.5 \text{ mA cm}^{-2}$ ,  $V_{OC} = 226 \text{ mV}$ ,  $FF = 0.34$ ,  $PCE = 0.50\%$ ), suggesting that the charge-separated state is long-lived. Little discussion was provided concerning the reason why these devices were so successful. Interestingly, it has a very similar structure to a previously reported dye; O2.<sup>60</sup>

**Figure 19.** Molecular structure of QT-1 and the structurally similar dye O2.<sup>58,60</sup>

**Figure 20.** Molecular structure of arylamine dyes with one or two anchors designed for p-DSCs reported by the group of Lin.<sup>59,61</sup>

When employed in a p-DSC, O2 performed only modestly ( $J_{SC} = 1.43 \text{ mA cm}^{-2}$ ,  $V_{OC} = 94 \text{ mV}$ ,  $FF = 0.37$ ,  $PCE = 0.05\%$ ).<sup>58</sup> This comparison highlights how fairly minor structural changes can have a large effect on device efficiencies. Lin and co-workers designed a series of arylamine-based dyes with a single acceptor unit and one or two carboxylic acid anchoring units to directly probe the effect of multiple anchoring sites on device

performances (Figure 20).<sup>59,61</sup> Comparing the two dyes with the 1,3-diethyl-thiobarbituric acid acceptor unit (Lin-1 and Lin-2), devices made with the multi-anchored dye out-performed those made with the single-anchored dye (Lin-1;  $J_{SC} = 1.38 \text{ mA cm}^{-2}$ ,  $V_{OC} = 113 \text{ mV}$ ,  $FF = 0.34$ ,  $PCE = 0.053\%$ , Lin-2;  $J_{SC} = 2.18 \text{ mA cm}^{-2}$ ,  $V_{OC} = 122 \text{ mV}$ ,  $FF = 0.35$ ,  $PCE = 0.092\%$ ). This improved performance was attributed to the second anchoring unit enhancing the binding strength between the dye and the semiconductor, thereby facilitating more efficient charge transfer. It was also suggested that the improvements were due to a suppression of the dark current of the device from more effective coverage of the NiO surface by the dye. However, a lower dye loading ( $1.54 \times 10^{-7} \text{ mol cm}^{-2}$  for Lin-1 vs.  $1.19 \times 10^{-7} \text{ mol cm}^{-2}$  for Lin-2) was observed for the dye containing two anchoring units.

**Figure 21.** Molecular structures of squaraines described in Warnan *et al.* Study.<sup>62</sup>

The same trend was seen for the squaraine dyes, with the double-anchored structure proving more efficient (p-SQ1;  $J_{SC} = 1.22 \text{ mA cm}^{-2}$ ,  $V_{OC} = 117 \text{ mV}$ ,  $FF = 0.37$ ,  $PCE = 0.053\%$ , p-SQ2;  $J_{SC} = 1.92 \text{ mA cm}^{-2}$ ,  $V_{OC} = 140 \text{ mV}$ ,  $FF = 0.42$ ,  $PCE = 0.113\%$ ). Again, the improvements were attributed to a suppression of the dark current. In comparison to the first report, here the dye with two anchoring units had a higher dye loading ( $1.98 \times 10^{-7} \text{ mol cm}^{-2}$  for p-SQ2 vs  $1.07 \times 10^{-7} \text{ mol cm}^{-2}$  for p-SQ1), possibly due to a more compact dye monolayer brought about from the more rigid anchoring mode. Warnan and co-workers also produced a series based on iodo-squaraines (SQ) (Figure 21).<sup>62</sup> SQ showed fast hole injection, however it suffered from subsequent fast recombination. A PMI unit was included to act as a light harvesting antenna and a secondary electron acceptor (SQ-PMI). Additionally, a terminal electron acceptor unit, NDI, was added to this system in an attempt to slow recombination further (SQ-PMI-NDI). The PCE of the systems steadily increased in the order of;  $SQ < SQ-PMI < PMI-NDI \ll SQ-PMI-NDI$ . The charge-separated state was extended long enough that a metal based redox mediator could be utilised, however the best device performance was achieved with iodine (SQ-PMI-NDI/  $I^-/I_3^-$ :  $J_{SC} = 2.73 \text{ mA cm}^{-2}$ ,  $V_{OC} = 95 \text{ mV}$ ,  $FF = 0.32$ ,  $PCE = 0.083\%$ ,  $Co^{II}/Co^{III}$ :  $J_{SC} = 1.17 \text{ mA cm}^{-2}$ ,  $V_{OC} = 175 \text{ mV}$ ,  $FF = 0.27$ ,  $PCE = 0.055\%$ ). The authors argued that novel squaraines based on push-pull systems containing an electron withdrawing moiety are required for future development.

Very recently a new series of triphenylamine dyes was reported by Brisse *et al* (Figure 22).<sup>63</sup> The new dyes are homologous to the benchmark P1. The authors tuned electron acceptor moiety with increasing electronic affinity in the series of four triphenylamine-bithiophene push-pull dyes in order to shift their absorption to the red region of the visible spectrum. With an iodine electrolyte, one of the dyes possessing a 1,3-diethyl-2-thiobarbituric acceptor gave a PCE reaching 0.124% and a  $J_{SC}$  of  $4.32 \text{ mA.cm}^{-2}$ .

**Figure 22.** Molecular structures of push-pull dyes synthesized by Brisse *et al.* (RBG-174, COCO, BBTX, COCN).<sup>63</sup>

**Figure 23.** Molecular structure of DPP-dyads used for p-DSCs.<sup>15,64,65</sup>

While triphenylamine-based push-pull dyes have dominated the p-DSC field since the work of Sun and Bach, very recently a publication by Odobel and co-workers described a highly efficient diketopyrrolopyrrole (DPP) dyad that does not contain an amine donor (Figure 23).<sup>15,25,42</sup> DPP dyes are attractive because of their numerous features, such as high photostability, electron withdrawing properties well-suited to reach high oxidizing power in the excited state, and straightforward synthesis. Th-DPP-NDI (Figure 23) had a modest extinction coefficient of  $37\,000\text{ dm}^3\text{ mol}^{-1}\text{ cm}^{-1}$ , lower than any of the other dyes that produced a high  $J_{SC}$ . Despite this the average  $J_{SC}$  of NiO/Th-DPP-NDI devices was  $7.38\text{ mA cm}^{-2}$  and the 'champion' device produced  $8.2\text{ mA cm}^{-2}$ , which is comparable to the record dyes CAD3 and QT-1. The NDI acceptor group is essential for these high performances, as Th-DPP produced only a negligible current response that could be attributed to the dye. It is possible that the success of this molecule will stimulate the design of more varied dyes for p-DSCs. These DPP dyes also serve as a prime example of how subtle structural modifications can have a significant effect on device performances. A DPP dyad with mixed phenyl/thiophene bridges (DPP-NDI) was previously reported by the same group and devices made using this dye obtained a  $J_{SC}$  of  $1.79\text{ mA cm}^{-2}$ . The lower  $J_{SC}$ , coupled with a lower  $V_{OC}$  ( $V_{OC} = 147$  and  $91\text{ mV}$  for Th-DPP-NDI and DPP-NDI respectively), resulted in a PCE that was seven times lower than Th-DPP-NDI (PCE = 0.35% and 0.048% for Th-DPP-NDI and DPP-NDI respectively).<sup>64,65</sup>

**Figure 24.** Molecular structures of the isoindigo dyes.<sup>66</sup>

Structurally similar to DPP-based sensitizers are isoindigo derivatives (Figure 24). In 2015, Odobel and co-workers investigated two indigo sensitizers for their novel application in NiO p-DSCs. A N,N-di(4-benzoic acid) phenylamine moiety acted as an anchoring (donor) group, and the isoindigo as the acceptor (ISO-Br) (Figure 24). It is worth mentioning that a second dye was produced which was additionally functionalised with an NDI unit (ISO-NDI). The dyes displayed a broad charge transfer band and an extended absorption ( $< 700\text{ nm}$ ), explaining their promising performances (ISO-Br/  $\text{Co}^{II/III}$ :  $J_{SC} = 0.80\text{ mA cm}^{-2}$ ,  $V_{OC} = 182\text{ mV}$ , FF = 0.23, PCE = 0.033, ISO-NDI/  $\text{Co}^{II/III}$ :  $J_{SC} = 1.54\text{ mA cm}^{-2}$ ,  $V_{OC} = 260\text{ mV}$ , FF = 0.25, PCE = 0.100%).<sup>66</sup> The performance and simplicity of these sensitizers opens up space for future development. Recently, a novel bay-annulated indigo (BAI) derivative has been reported (Figure 25), producing a promising photocurrent ( $I^-/I_3^-$ :  $J_{SC} = 1.14\text{ mA cm}^{-2}$ ).<sup>67</sup>

**Figure 25.** Molecular structure of BAI-COOH.<sup>66</sup>

Furthermore, a novel series of triphenylamino-free pyran-based dyes (Figure 26) have been prepared in which the performance of CB7 and CB8 exceeded, in the reported conditions, that of the benchmark P1 (CB7:  $J_{SC} = 2.00\text{ mA cm}^{-2}$ , PCE = 0.076%, CB8:  $J_{SC} = 1.72\text{ mA cm}^{-2}$ , PCE = 0.066, P1:  $J_{SC} = 1.66\text{ mA cm}^{-2}$ , PCE = 0.064).<sup>78</sup> CB8 was found to absorb in the higher regions of the visible spectrum making it an ideal candidate for t-DSCs.

This survey of the literature reveals that consistently, the most promising dyes are those with charge-transfer character, such as the triphenyl amine push-pull dyes and molecular dyads such as Th-DPP-NDI. It can be challenging to compare directly the performance unless a benchmark, such as P1, is used because of the variation in NiO quality between research groups. Generally, symmetrical dyes with two acceptors are beneficial in terms of strong light absorption (and high  $J_{SC}$ ), whereas having only one acceptor but two anchoring groups is beneficial in terms of stability and protecting the surface (high  $V_{OC}$ ). The lifetime for charge-separation (see section 3) is improved by positioning the acceptor away from the metal oxide surface, compared to dyes without a donor-acceptor structure, however, the charge-separated state lifetimes of dyes on NiO still lag orders of magnitude lower than dyes on  $\text{TiO}_2$ . PMI-6T-TPA, which combines the best features of all the dyes, in conjunction with iron acetylacetonate, has reached the highest efficiency for a p-type DSC (ca. 2.5%) to date.

**Figure 26.** Molecular structure of triphenylamino-free pyran-based dyes.<sup>78</sup>

### 2.3 Porphyrin and Bodipy sensitizers

**Figure 27.** Molecular structure of porphyrins synthesised and tested in p-DSCs; ZnP and ZnP-NDI reported by Odobel *et al.*; ZnTCPP and  $\text{C}_{60}\text{PPy}$  reported by Tian *et al.*<sup>67,69</sup>

**Figure 28.** Chemical structure of the porphyrins studied by Gibson *et al.*<sup>75</sup>

Beyond the widely researched ruthenium and triphenylamine-based push-pull sensitizers, there have been other unique developments focusing on porphyrin and bodipy dyes. While porphyrins remain one of the most effective and researched molecules in n-DSCs, their application in p-DSCs hasn't received as much attention. This is possibly due to the dissatisfactory efficiencies reported in early papers, for example He and co-workers found that the free base tetrakis(4-carboxyphenyl) porphyrin (TCPP) gave a PCE of only 0.003%.<sup>13</sup> Odobel *et al.* attempted to improve the performance by applying an electron accepting phosphorus porphyrin in p-DSCs. While this approach is logical, the solar cell performance was disappointing (IPCE = ca. 2.5 %). Inspection of the relative redox potentials indicate that while the driving force for photoinduced charge-separation was very favourable,  $\Delta G^0 = -1.1\text{ eV}$ , the low-lying reduction potential ( $-0.6\text{ V vs. SCE}$ ) meant that the driving force for

regeneration was insufficient for regeneration of the dye to compete with charge-recombination.

More electron donating zinc porphyrin based dyes (Figure 27) have given modest results (for ZnP,  $J_{SC} = 0.19 \text{ mA cm}^{-2}$ ,  $V_{OC} = 98 \text{ mV}$ ,  $\eta = 0.006\%$ ; for ZnTCPP,  $J_{SC} = 0.5 \text{ mA cm}^{-2}$ ,  $V_{OC} = 120 \text{ mV}$ ,  $FF = 40\%$ ,  $\eta = 0.02\%$ ).<sup>68,69</sup> It has been postulated that the limiting factor in the zinc porphyrin system was fast electron-hole recombination at the interface between the dye and the NiO. Appending an NDI electron acceptor to ZnP improved the p-DSC performance (ZnP-NDI  $J_{SC} = 1.38 \text{ mA cm}^{-2}$ ,  $V_{OC} = 127 \text{ mV}$ ,  $FF = 32\%$ ,  $\eta = 0.012\%$ ).<sup>70</sup> Likewise, Tian also tested a supramolecular system with ZnTCPP coordinated to N-methyl-2-(4'-pyridyl)-3,4-fulleropyrrolidine ( $C_{60}$ PPy).<sup>69</sup> This design was inspired by previous reports of supramolecular interactions between porphyrins and  $C_{60}$  derivatives, which showed a fast porphyrin to  $C_{60}$  charge transfer process and a long lifetime for the reduced fullerene.<sup>73,74</sup> NiO films sensitized using ZnTCPP/ $C_{60}$ PPy performed more efficiently than the porphyrin alone ( $J_{SC} = 1.5 \text{ mA cm}^{-2}$ ,  $V_{OC} = 158 \text{ mV}$ ,  $FF = 38\%$ ,  $\eta = 0.09\%$ ). The authors attributed this increased performance to a suppression of recombination between the reduced dye and NiO. The authors recommended that a new anchoring group, spacer units and the introduction of a novel electron acceptor are pertinent for future optimization. Recently, Gibson et al. demonstrated the efficient employment of click chemistry to synthesise a new porphyrin with a coumarin anchor group (3, Figure 28) which augments binding stability.<sup>75</sup> This system was efficiently coupled with a  $C_{60}$  acceptor following the approach by Tian et al.<sup>69</sup> The efficiencies obtained were low but comparable (around 0.02%).

**Figure 29.** Molecular structure of 1-7 and 4,4-difluoro-8-(4-carboxyphenyl)-1,3,5,7-tetramethyl-2,6-diethyl-3a,4a-diaza-4-bora-s-indacene (Bodipy-CO<sub>2</sub>H) investigated as NiO photosensitizers.<sup>76,77</sup>

Boradiazaindacene (bodipy) dyes are popular in a range of applications but have been used infrequently and with moderate success in n-DSCs. However, their large extinction coefficients, electrochemical stability and tuneable absorption properties (i.e. to optically match photoanodes in tandem cells) prompted Lefebvre and co-workers to choose a bodipy dye for p-type DSC tests.<sup>75</sup> The applicability of boradiazaindacene (bodipy) dyes for promoting charge-separation was successfully demonstrated. The triphenylamine donor-bodipy acceptor produced an impressive  $J_{SC}$  ( $3.15 \text{ mA cm}^{-2}$ ) which was at the time comparably superior to related triphenylamine-based dyes.<sup>76</sup> Later, a series of triphenylamine donor-based bodipy dyes appending a carboxylic acid anchoring group and thiophene spacers were investigated (Bodipy-CO<sub>2</sub>H). A positive effect on PCE was observed upon addition of thiophene spacer units. Less substituted bodipy dyes (5 and 7, Figure 29) showed higher IPCE comparative to the hindered dyes 4 and 6 (IPCE 4 = 27%, 7 = 53%). A higher  $J_{SC}$  ( $5.87 \text{ mA cm}^{-2}$ ) was reported for Bodipy 7 and was accredited to an improved electronic communication with NiO.<sup>77</sup>

Besides the broad use of porphyrins for n-type DSCs and optimization of such dyes carried out by different research groups, they seem, so far, to be less promising for applications in p-type cells. A possible approach to improve the performance would be to build in a push-pull design and to improve the orbital overlap between the HOMO on the dye and states in the NiO valence band. However, the synthesis of asymmetric porphyrins is typically limited by low yields and multiple steps. Bodipy dyes are relatively more straightforward to synthesise and have reached current densities which are almost comparable with the push-pull dyes described above (ca. 0.3%). The field concerning bodipy based sensitizers is growing and is still open to optimization, possibly by developing dyad systems with an acceptor unit such as  $C_{60}$ .

### 3. Kinetics

#### 3.1 The dye-semiconductor interface

**Figure 30.** Energy level diagram of the backward processes in a p-type nickel oxide dye-sensitized solar cell with an iodide/triiodide redox couple. 1) Dye relaxation; 2) dye- $|NiO^+$  recombination; 3) electrolyte- $|NiO^+$  recombination.

In order to gain a deep insight into the mechanisms that regulate the incident photon to current conversion (IPCE) of p-type DSCs with different sensitizers, transient absorption spectroscopy (TAS) and transient infrared spectroscopy (TR) can be employed. TAS is typically applied to study the ultrafast dynamics, which is made possible because the injection, recombination and relaxation pathways occur on very different timescales, with characteristic rate constants. The undesirable excited state relaxation and charge-recombination processes in p-type systems are shown in Figure 30. The fate of an electron in a dye-sensitized solar cell is determined by kinetic competition between charge separation and recombination processes. The typical lifetimes associated with these processes are given in Figure 31. For characteristic NiO systems, charge-injection is a fast process, between 100 femtoseconds to 100 picoseconds.<sup>20</sup> However, dye- $|NiO^+$  recombination generally occurs on a picosecond to nanosecond timescale and is often, but not always, measured to be faster than regeneration which has been reported from nanosecond up to microsecond timescales, leading to an inefficient solar cell.<sup>76,79</sup> Elaborate donor-acceptor dyes can give charge-separated state lifetimes of up to microseconds.<sup>80-82</sup> Fast charge-recombination may be a result of the low hole mobility of NiO or the electronic vacancies which exist above the valence band edge.<sup>83</sup> Furthermore, whereas charge transport through TiO<sub>2</sub> is believed to be diffusive, for NiO a hole-hopping mechanism at the NiO/electrolyte interface has been proposed, which may also promote semiconductor/electrolyte recombination.<sup>21,84</sup> This hopping mechanism for NiO is believed to originate from 'trap states' caused by the presence of  $Ni^{3+}$  and  $Ni^{4+}$ .<sup>83,85</sup>

**Figure 31.** Energy level diagram of the components within a dye-sensitized solar cell with the relevant timescales of each process in p-type NiO.

Most studies on the dynamics of photoinduced electron transfer from mesoporous NiO to an excited dye molecule bound to the surface were reported by Hagfeldt and co-workers.<sup>86</sup> In this work, C343-sensitized NiO was chosen as a model system to study interfacial electron-transfer dynamics. The kinetic processes were found to be multi exponential and a major ultrafast component ( $\sim 200$  fs) was present, which is of the same order of magnitude as the time constants measured for photoinduced electron injection in C343-TiO<sub>2</sub> colloid solutions. However, back electron transfer, which is also multi exponential, is remarkably fast, with the main part of the recombination process occurring with a time constant of  $\sim 20$  ps. In Table 1, dye structures and their corresponding dye<sup>-</sup>|NiO<sup>+</sup> charge-separated state lifetimes are shown for all p-type nickel oxide systems, where this information was reported. Charge-recombination is generally believed to occur over a range of timescales due to holes being present in different environments in the nano-particulate film, so in some cases multiple lifetimes are attributed to this process.

Long-lived (microsecond) charge-separated state lifetimes on nickel oxide have been observed for some metal complexes, such as [Ru(dcb)<sub>2</sub>(NMI-phen)]<sup>2+</sup> (namely bis-(2,2'-bipyridine-4,4'-dicarboxylic acid)<sub>2</sub> N-(1,10-phenanthroline)-4-nitronaphthalene-1,8-dicarboximide ruthenium(II)) (Figure 32).<sup>33,87</sup> The presence of the electron-accepting group, 4-nitronaphthalene-1,8-dicarboximide (NMI), attached to the phenanthroline of [Ru(dcb)<sub>2</sub>(NMI-phen)]<sup>2+</sup> resulted in long-lived charge separation of the order of 10–50  $\mu$ s between reduced [Ru(dcb)<sub>2</sub>(NMI-phen)]<sup>2+</sup> and NiO valence band holes. Also, among iridium-based complexes, three sensitizers (IrPhen, IrDQC2, IrBpstyryl) were found to present a long-lived charge separated state of the order of the microsecond timescale.

**Figure 32.** Molecular structure of [Ru(dcb)<sub>2</sub>(NMI-phen)]<sup>2+</sup> dye.<sup>87</sup>

Organic molecules with an appended acceptor unit (A) also present a longer charge separated state lifetime than just the chromophore. Appending an electron acceptor (A) to the sensitizer (S), increasing the separation distance between the charges (hole in the valence band of NiO and electron on the sensitizer), leads to slower charge recombination at the dye<sup>-</sup>|NiO<sup>+</sup> interface. In some reported examples, the charge separated state was successfully increased by several orders of magnitude using this approach and some of the most efficient sensitizers for NiO are dyads of the type S–A. For example, Odobel et al. studied the photophysical properties of a perylene monoimide (PMI) dye connected to a naphthalene diimide (NDI) or a fullerene (C<sub>60</sub>) acceptor units. They reported a study of free dyads (PMI–Ph-NDI, PMI–PhC<sub>60</sub> and PMI–NDI).<sup>37</sup>

The proposed mechanism of hole injection for these dyads, PMI–A, starts with hole injection from the singlet excited state (<sup>1</sup>\*PMI), after photon absorption, and is followed by a charge shift reaction to A forming the final charge separated state A<sup>-</sup>|PMI|NiO<sup>+</sup>. The fast electron shift from the sensitizer to the acceptor is crucial to compete with the fast recombination

reaction. When bound to nanoporous NiO films, all the dyads presented in the study, exhibit ultrafast ( $\tau = 0.3\text{--}3$  ps) hole injection from the excited PMI unit to the NiO valence band. Transient absorption measurements show that the radical anion of the PMI unit is formed and undergoes charge shift to the acceptor unit (NDI or C<sub>60</sub>), which localizes the electron at a longer distance from the NiO surface.<sup>38</sup> The resulting charge separated state is long-lived, recombining on the ms timescale, which is a significant improvement compared to the recombination rate recorded with PMI-only based sensitizers. Both PMI–NDI|NiO and PMI–PhC<sub>60</sub>|NiO exhibit rapid ( $\tau = 2\text{--}20$  ps) formation of the final charge separated state A<sup>-</sup>|PMI|NiO<sup>+</sup> that competes favourably with recombination, resulting in charge shift yields greater than 80%. The electron transfer cascade in PMI–Ph-NDI|NiO shows more complex kinetics that compete with recombination and only achieves a 50% yield for NDI<sup>-</sup>.

The positive effect of NDI as an electron acceptor unit was also demonstrated in a more recent work by Odobel et al.<sup>13</sup> The investigators synthesised a new series of diketopyrrolopyrrole (DPP) dyes. The effect of appending a naphthalene diimine unit (NDI) as a secondary electron acceptor, in conjunction with the DPP, was analysed by transient absorption spectroscopy, which indicated that very fast charge-transfer lead to a hole injection quantum yield approximately close to unity for all the dyes. In contrast, the charge recombination rate constants differed substantially between the dyes with and without the NDI substituent. The latter exhibit a long-lived charge separated state of the order of one hundred microseconds. As a result, the dyes containing an NDI electron acceptor give superior photovoltaic performances.

The same strategy was applied to the design of porphyrin dyes and squaraines. Porphyrin-C<sub>60</sub> dyads have been widely studied and recently these systems have been explored by Tian et al. in p-type DSCs (see section 2).<sup>69</sup> The dynamics of charge-separation between a C<sub>60</sub> acceptor coordinated through the Zn centre of a porphyrin have been investigated by Gibson et al. using transient absorption spectroscopy to evaluate the effect of the electron acceptor on the charge-separated state lifetime. In this system, coordinating the zinc to a pyridyl-functionalised fullerene (C<sub>60</sub>PPy) extended the charge-separated state lifetime of porphyrin from *ca.* 200 ps to nanoseconds.<sup>75</sup> Similarly, Odobel and co-workers added the terminal electron acceptor unit NDI to a squaraine dye (SQ-PMI) to slow recombination (SQ-PMI-NDI).<sup>59</sup> Consequently, the PCE of the systems steadily increased in the order of SQ-PMI < SQ-PMI-NDI, obtaining a charge separated state of the order of microseconds.

More generally, the push-pull design has been shown to slow the rate of charge-recombination by moving electron density in the dye away from the nickel oxide surface towards the acceptor groups and the interface with the redox electrolyte. In these systems the anchor group is attached at the donor to locate the acceptor group furthest from the surface when adsorbed on nickel oxide, which is the opposite structure to push-pull dyes for n-type TiO<sub>2</sub> systems where the anchor is located near to the acceptor group. Time-resolved infrared spectroscopy has been particularly useful in probing the change

in electronic structure in dyes adsorbed on NiO, following light absorption. This technique probes changes in bond strength following laser excitation and has been previously applied to analyse charge transfer dynamics for dyes containing metal-carbonyl bonds adsorbed on TiO<sub>2</sub> films.<sup>90,91</sup> The nitrile acceptor in P1, which has a characteristic frequency of ~2000 cm<sup>-1</sup> is an excellent reporting unit for the excitation and subsequent reduction of P1.<sup>93</sup> The lifetimes extracted from TRIR experiments were consistent with femtosecond transient optical absorption spectroscopy of P1 adsorbed on the surface of NiO films, which revealed a rapid injection rate ( $\tau < 1$  ps), but a short charge-separated state lifetime ( $\tau < 1$  ns).<sup>23</sup>

PMI-6T-TPA, like P1, contains a triphenylamine electron donor, but is substantially larger in size compared to P1, partly due to the long, extended thiophene bridge, in addition to a perylene monoimide (PMI) chromophore, which is a good electron acceptor in the excited state. The importance of such extended linkers in terms of the charge-transfer dynamics was introduced by Bach et al.<sup>42</sup> The investigators studied the impact of systematically varying the length of the oligo-3-hexylthiophene bridge, which provides control over the spatial separation of the photogenerated charge carriers, from a bithiophene (n=1) to a quaterthiophene (n=2) and a sexithiophene (n=3). The results from transient absorption spectroscopy demonstrated a clear correlation between the length of the oligothiophene linker and the observed recombination kinetics. The champion dye with the sexithiophene bridge (PMI-6T-TPA) was associated with slower recombination kinetics with respect to the others (*ca.* 14  $\mu$ s). Assuming a similar molecular orientation of compounds, an increasing length of the oligothiophene bridge translates into an increased tunnelling distance between the electron occupying the dye's LUMO and the vacancies located in the NiO electrode, leading to a lower recombination rate. Similarly, Wu *et al.* reported a series of triphenylamine (TPA)-oligothiophene-perylenemonoimide molecules, denoted as the BH dyes.<sup>56</sup> They systematically studied the photophysical properties of the BH series of molecules with  $\pi$ -linkers of various lengths in solution via time-resolved absorption spectroscopy. When the BH dye attached onto the NiO films, ultrafast hole injection was observed within the instrument response time (<200 fs) as well as the slow injection component. They found that the recombination lifetimes span a remarkably wide time scale from tens of picoseconds to several microseconds. These results were consistent with Bach et al. in showing that varying the number of  $\pi$ -linkers to increase the spatial distance between the PMI units and holes in the NiO leads to a slower rate of charge-recombination.

Gibson et al. attempted to slow charge-recombination by varying the coupling between the chromophore and the thiophene bridge in a series of boron dipyrromethene (bodipy)-triphenylamine dyes. Transient absorption spectroscopy of 6 (Figure 29), a bodipy analogue of P1 where the acceptor is electronically decoupled from the thiophene linker, revealed the formation of a long-lived charge-separated state on nickel oxide ( $\tau = 180$  ns). Surprisingly, however, the solar cell performance, particularly IPCE, was lower for 6 than for the benchmark dye, P1.<sup>77</sup> This is possibly a consequence of

positioning the bodipy chromophore further from the NiO surface and slowing down the initial charge-separation process. By comparison, dye 7, a derivative with greater electronic coupling with the thiophene, was shown to have a much shorter charge-separated state lifetime but generated considerably more photocurrent than dye 6.<sup>77</sup>

Generally, these studies support the strategies of donor-acceptor dye designs and spatial separation from the semiconductor NiO surface to retard the charge recombination processes. However, there still remains quite a gap in fundamental understanding on the dynamics of charge-transfer at the interface between dyes and p-type metal oxides such as NiO. Clearly there is a discrepancy between the measured dynamics of sensitized films and the performance of the photoelectrodes in complete devices. For a high quantum efficiency, at least an order of magnitude difference between the lifetime with and without electrolyte is required, and typically charge-separated state lifetimes of the order of microseconds are observed with n-type devices.<sup>90</sup> Indeed, in the case of sensitized semiconductor based photoanodes, the quantum yield can be expressed as the product of three terms related to the key steps of the device working principle:

$$IPCE = LHE\phi_{inj}\eta \quad (\text{Eq.1})$$

where *LHE* is the light harvesting efficiency,  $\phi_{inj}$  is the electron injection (from sensitizer to semiconductor) quantum yield and  $\eta$  is the efficiency of *e*<sup>-</sup> collected at the photoanode. Being efficiency dependent on electron collection, quantum yield can be represented as a ratio between the rate constants of forward (electron collection) and reverse processes (electron recombination). Therefore, if the charge-separated lifetimes are short (< ns), theoretically, the liquid-junction cell should not work. Nonetheless, dyes such as P1 and CAD3<sup>92</sup>, which have a relatively short charge-separated state lifetimes (*ca.* < 10 ns), still generate relatively high photocurrents in NiO dye-sensitized solar cells.

As previously mentioned, time-resolved absorption spectroscopy experiments on films in the presence of a solution of iodine and lithium iodide, showed that the charge-separated state decays over a longer timescale than in the presence of an inert electrolyte, which could suggest that species in the electrolyte associate with the cationic dyes adsorbed on nickel oxide or species on the surface of NiO. This association slows recombination (extending the lifetime of the dye radical anion) rather than the expected increase in the rate of regeneration (quenching the lifetime of the dye-radical anion), and the effect is attributed to the promotion of the reaction between I<sup>-</sup> and Ni<sup>3+</sup>. Indeed, as discussed in section 3, charge-recombination has been associated with the presence of Ni<sup>3+</sup> states, and it has been demonstrated that the electrolyte chemically reacts with the NiO surface, whereby I<sup>-</sup> reduces the Ni<sup>3+</sup> states.<sup>85,89</sup>

### 3.2 The semiconductor-electrolyte interface

Other techniques have been employed to evaluate the dynamics of slower processes in dye-sensitized photocathodes,

such as charge transport and charge recombination at the NiO|electrolyte interface, including photocurrent and photovoltage transient measurements and electrochemical impedance spectroscopy.

Hagfeldt *et al.* reported the first investigation of hole diffusion length in p-DSCs incorporating mesoporous NiO electrodes.<sup>94</sup> In their study, time constants for charge-transport and charge-lifetime were obtained from small light-modulation transient photocurrent measurements under short-circuit conditions and open circuit voltage transients. Despite the slower charge-diffusion rate in NiO compared to TiO<sub>2</sub>, it was noticed that at low light intensities, hole lifetimes ( $\tau_h$ ), which are measured at open circuit, are much larger than hole transport times ( $\tau_{tr}$ ), which are measured at short circuit. These two values, at the same equivalent light intensity or charge-density, can be associated directly to the charge collection efficiency,  $\eta_{cc}$  that can be estimated as:

$$\eta_{cc} = 1 - \frac{\tau_{tr}}{\tau_h} \quad (\text{Eq.2})$$

Furthermore, the study revealed that mesoporous NiO displays a transport time that is almost independent from light intensity and is strongly dependent on the type of cation in the electrolyte. This was attributed to adsorption of the cations affecting the hopping of charge at the NiO|electrolyte interface, supporting the idea that the holes are Ni(III) sites at the surface. However, hole lifetimes were found to decrease sharply with increasing light intensity, as a higher charge density is expected to lead to an increase in recombination. It is interesting that charge transport in NiO is not affected by concentration of charge, keeping a relatively constant diffusion coefficient until high bias light intensities.<sup>95,96</sup>

Following this report several studies on hole transport properties of NiO have been carried out. Mori *et al.* determined an apparent diffusion coefficient:

$$D = \frac{d^2}{2.77\tau_h} \quad (\text{Eq.3})$$

(where  $d$  is the film thickness) of  $5 \times 10^{-8} \text{ cm}^2 \text{ s}^{-1}$ , while Hagfeldt *et al.* obtained a diffusion coefficient that is 3 times larger, by modifying the NiO preparation route.<sup>96,97</sup> This result demonstrated that the diffusion property of NiO can be easily tuned by changing the film preparation. Transient measurements were also employed to analyse the effect of doping, of applying an insulating blocking layer and of varying the redox mediator on the hole lifetime and transport time.<sup>38,98-100</sup> Hagfeldt *et al.* measured the hole lifetime and transport times of devices employing several cobalt-based redox mediators. Consistent with previous observations, the hole lifetimes were strongly dependent on light intensity, whereas the hole transport times were independent of light intensity (unless the hole lifetime became sufficiently short to affect the measurement). At the same time, while the transport times were found to be almost independent from the cobalt complexes used in the devices, the lifetimes were strongly dependent on the steric bulk of the cobalt polypyridyl ligand (see section 4). Furthermore, Odobel *et al.* found that with  $I_3^-/I^-$

the hole lifetime is shorter than with the Co<sup>III/II</sup> redox couple studied.<sup>38</sup> They attribute the relatively long hole lifetimes in the presence of the cobalt species to the large steric bulk of the tertiary-butyl substituents on the bipyridyl ligands, which increase the distance between the NiO and the cobalt centre.

Photocurrent and photovoltage transients have also employed to compare charge lifetime and transport on NiO sensitized with different dyes, for example the CAD dye series, in which the steric properties of the dyes were varied. Devices utilizing CAD2 and CAD3, have charge lifetimes that are notably longer than those utilizing CAD1, confirming that the bulky alkyl substituents on the periphery of the dye inhibit charge-recombination between the NiO and the redox couple.<sup>51</sup> Furthermore, it was found that CAD2 and CAD3 exhibit charge lifetimes comparable to those of previously studied dyes such as P1.<sup>37,41</sup>

Charge recombination and charge-transport can also be studied using electrochemical impedance spectroscopy (EIS). Electrochemical impedance spectroscopy is a frequency-domain approach which measures current response to the application of an AC voltage as a function of frequency.<sup>101,115</sup> Generally for n-type DSCs, Nyquist diagrams under illumination typically feature three semicircles, assigned to the charge transfer process at the platinized counter electrode (in the range of kHz), the transport and recombination of the photoinjected electrons in the porous TiO<sub>2</sub> film (in the range of 1-100 Hz), and Nernst diffusion within the electrolyte (in the range of mHz), respectively.<sup>102,103</sup>

Wu *et al.* reported a systematic and fundamental study of the impedance spectra of NiO p-DSCs. Nyquist plots featuring two semicircles were observed. By fitting the data to the standard equivalent circuit model, the kinetic processes were separated, and key parameters were extracted, including the charge recombination resistance, chemical capacitance, and hole lifetime. The first semicircle (Figure 33) was assigned to the charge transfer reaction at the electrolyte/counter electrode interface, while the second semicircle was assigned to the recombination charge transfer process at the NiO/dye/electrolyte interface. The hole lifetime ( $\tau$ ) was calculated by:

$$\tau = R_{rec}C_{\mu} \quad (\text{Eq.4})$$

Where  $R_{rec}$  is recombination resistance and  $C_{\mu}$  is associated capacitance. It was found that hole lifetimes obtained by their EIS measurement were comparable to those obtained by other methods.<sup>99</sup>

Wu *et al.* also applied EIS to investigate the reasons behind the low fill factor (FF) in p-DSCs.<sup>104</sup> Previously, Cheng *et al.* proposed that the short hole diffusion length and insufficient charge collection determined by charge recombination at electrolyte-electrode interface might account for the relatively low FF.<sup>105</sup> Whereas, Wu *et al.* suggested that the low fill factor value is largely attenuated by the recombination of holes in NiO with the reduced dyes. Indeed,  $R_{rct}$  is affected by both  $R_{rct-el}$  and  $R_{rct-dye}$ , with the latter process dominating under the SC condition. As matter of fact, the lower dielectric constant of NiO

means NiO is less effective in screening the Coulombic interaction between the charged dye and the charge carriers in the semiconductor compared to TiO<sub>2</sub>. Furthermore, they observed that the large values of C<sub>μ</sub> can be associated to a surface charging/hopping mechanism for the storage/transport of holes in NiO. These considerations were supported by a more recent work by Bach and co-workers which attributed efficiency losses to fast recombination with dye and as the main reason associated to a poor FF, along with poor hole injection efficiency (Φ<sub>inj</sub>), under applied bias.<sup>106</sup>

However, Zaban et al. highlighted hole transport as the performance limiting factor of p-DSCs. Their impedance results shed light on the fact that hole transport in the mesoporous film is a limiting factor to the performance of the solar cell, pointing out the need to improve the hole conductivity of the NiO based electrode.<sup>107</sup> Once understood the dynamics that regulate the PCE of p-type DSCs, the same technique was used to evaluate strategies to improve the efficiency such as treatment of the NiO surface, doping or the use of a suitable blocking layer (see section 5) and to gain a deep insight into comparisons of different electrolytes and sensitizers.

**Figure 33.** (top) Equivalent circuit of NiO p-DSC where R<sub>s</sub> is the equivalent series resistance of the device, parallel RC units model the various interfaces and a Warburg element models electrolyte diffusion. (bottom) Nyquist plot of cell at open circuit under 1 sun illumination. The red solid line shows the fitting curve.<sup>104</sup>

Li et al. reported a simple Ni(CH<sub>3</sub>COO)<sub>2</sub> post-treatment method, which the authors propose, can offer an effective way of decreasing the surface NiO(OH) structure, resulting in diminishing the hole recombination, increasing the charge collection efficiency, leading to a 31.3% improvement in the photovoltaic performance.<sup>108</sup> The charge collection efficiency (η<sub>cc</sub>), obtained by EIS, which is related to the ratio of charge transport through NiO and charge recombination, can be calculated by the following equation:

$$\eta_{cc} = 1 - \left( \frac{R_t}{R_h} \right) * C_{\mu} \quad (\text{Eq.5})$$

The η<sub>cc</sub> was found to be higher for post-treated devices. This observed electrochemical character of treated sample was attributed to the decrease of surface defects (species NiO(OH)) by Ni(CH<sub>3</sub>COO)<sub>2</sub> treatment, which can inhibit back hole transfer from the NiO to electrolyte.<sup>108</sup>

Wu et al. doped NiO with different quantities of CoO. From EIS measurements they found out that the τ<sub>r</sub> increased from ~5 ms for p-DSCs assembled with pure NiO cell by more than 2-fold for 2% and 6% Co-doped NiO films. The authors attributed this to the dopant ions acting as scattering centres for the electrons or holes, reducing the probability of polaron hopping and reducing the hole and electron mobility values. The V<sub>oc</sub> increased from 122 mV up to a maximum of 158 mV with > 6% cobalt doping. This was consistent with the lowering of the flat-band potential (observed from Mott-Schottky measurements) of the NiO by a few tens of mV and to higher hole lifetimes for the Co-doped

cells than those for pure NiO cells.<sup>109</sup> Meanwhile, lithium as dopant was found to improve the electrical properties of the films. The EIS analysis clarified that this behaviour is due to a strong dependence of the valence band shape and position with respect to the Li-doping concentration. Hammarström et al. demonstrated evidence that the decreased recombination of Li-doped NiO DSCs is attributed to a downward shift of the valence band, which increases the energy barrier for interface recombination. Another reason results in narrowing the trap energy distribution of Li-doped NiO photoelectrodes which can weaken energy overlap with the LUMO level of dye and subsequently the recombination path of hole back transfer to the dye is hindered.<sup>116</sup>

At the same time, with alumina as blocking layer, Wu et al. showed a higher recombination resistance value from the electrochemical impedance studies. It has thus been established that the increase in V<sub>oc</sub> upon alumina treatment arises due to a higher resistance for electron/hole recombination across the NiO surface, locally.<sup>110</sup> Meanwhile, spray pyrolysis of TiO<sub>2</sub> on NiO was found to increase recombination resistance.<sup>111</sup> The τ<sub>r</sub> was calculated from the recombination resistance and the chemical capacitance. The results showed that TiO<sub>2</sub> treated devices exhibited the longest hole lifetime, leading to a higher hole density, a higher Fermi level and, therefore, a higher V<sub>oc</sub> and PCE. Similar behaviour was found studying the effect of a NiO blocking layer through electrochemical impedance spectroscopy, which demonstrated that charge recombination was suppressed pointing to a higher photocurrent and fill factor.<sup>112</sup>

The effect of recombination suppression for a series of dyes in which the structure was systematically varied, has also been evaluated using EIS analysis. As an example, impedance spectroscopy revealed that zxx-op1-2 exhibits a longer hole lifetime, and a higher photogenerated hole density than zxx-op1 and zxx-op1-3. All results indicated that the dye zxx-op1-2 formed a much more compact dye block layer than zxx-op1 and zxx-op1-3, with regard to retarding the charge recombination between the injected hole in the NiO film and the hole acceptor in the electrolyte, leading to better performance.<sup>50</sup> The same approach was employed for the study of zxx-op2 and zxx-op3 dyes and a family of squaraines (SQ).<sup>51,112</sup>

The effect of the electrolyte composition was also screened by EIS measurement: the influence of the presence of an additive such as chenodeoxycholic acid was evaluated by Odobel and co-workers.<sup>113</sup> Analysis of electrochemical impedance spectroscopy provides evidence that the role of the CDCA layer is to create a physical barrier to prevent the approach of the redox mediator from the NiO surface and consequently raise the open circuit voltage, as demonstrated by higher hole lifetimes in the presence of such additive.

At the same time the technique was used to study semiconductor materials as alternatives to the conventional NiO substrate (see section 5). Guldi and co-workers reported a study about the detailed optimization of CuO-DSCs by combining device analysis with a comprehensive electrochemical impedance spectroscopic (EIS) study.<sup>114</sup> They evaluated the impact of the CuO electrode fabrication, e.g.

calcination temperature and electrode thickness, and the  $I^-/I_3^-$  electrolyte ratio on the device performance. They studied the effect of different device parameters on  $R_{CT}$  in concert with advanced EIS parameters  $\eta_{cc}$ ,  $D$  and  $\tau_h$  as a function of calcination temperature, electrode thickness, and electrolyte ratio. A calcination temperature of 300 °C and a film thickness of 5.0  $\mu\text{m}$  yielded the best balance between dye loading, charge injection, and recombination, with an optimum  $I^-/I_3^-$  electrolyte ratio of 2.5:1 for the dye regeneration process. In addition, the effect of trap states on the  $\tau_h$  has been studied for the first time in p-type DSCs by EIS. For the above-mentioned variables different observations have been obtained. In the context of sintering temperature and the electrode thickness, large differences in  $C_\mu$  were governing  $\tau_h$ , which led to longer lifetimes and increased recombination for a higher amount of trapping. For the different electrolyte molar ratios, the differences in  $C_\mu$  were small and, thus,  $R_{CT}$  showed a major impact on  $\tau_h$ . Here, a shorter lifetime pointed to a faster recombination of the trapped charge carriers. Furthermore, the reactivity of non-sensitized CuO electrodes with the electrolyte solution was probed by EIS measurements in the dark and compared to state-of-the-art NiO electrodes. Surprisingly, CuO electrodes showed a lower reactivity towards the redox couple compared to NiO electrodes.

Generally, dynamic studies using EIS and transient photovoltage and photocurrent decay measurements have demonstrated that there is a pronounced correlation between PCE and both suppressing charge recombination and enhancing charge transport, which can be tuned by modifying the semiconductor properties, electrolyte and dye design.

#### 4 Electrolytes

**Figure 34.** Molecular structure of PCBM.<sup>118,117</sup>

**Figure 35.** Molecular structures of the oxidized (5,50 -dithiobis(1-phenyl-1H-tetrazole)) and reduced (sodium 1-phenyl-1H-tetrazole-5-thiolate) forms of the redox couple.<sup>120</sup>

In a DSC, the electrolyte is responsible for regenerating the ground state of the dye and transporting electrons to the counter electrode. Its optimization is crucial, therefore, for the design of tandem devices. Most p-DSCs use a liquid electrolyte, which is typically  $I^-/I_3^-$  or a metal complex-based redox shuttle, but recently a few solid-state p-DSCs have been reported.<sup>116,117</sup> In this context, phenyl- $C_{61}$ -butyric acid methyl ester (PCBM), instead of liquid redox couple electrolyte, has been employed as a solid electron-transfer material (Figure 34). Tian et al. reported the first example of a p-type solid state dye sensitized solar cell (p-ssDSC).<sup>117</sup> The photovoltaic data support the feasibility of the concept, but the PCE of the device was low. This was attributed to the short lifetime of the reduced dye (P1) on the NiO surface and slow dye regeneration from PCBM. Odobel *et al.* improved the p-type DSC performance by substituting the P1 dye with a simple DPP

(diketopyrrolopyrrole) dye bearing a thienyl carboxylic acid as binding group and a derivative<sup>118</sup>, which was furnished with a pyromellitimide (PYRO) group acting as a secondary inner electron acceptor. The performance of this kind of device still lags below devices prepared with liquid electrolytes however.

The most common liquid electrolyte is  $I^-/I_3^-$  (typically formed from a solution of  $I^-$  and  $I_2$  in acetonitrile) and this has been used for many high-efficiency devices.<sup>45,48</sup> The iodine-based electrolyte composition has been optimised for the p-type system by changing the solvent and the additives.<sup>89,119</sup> However, despite its widespread use, there are several drawbacks connected to this electrolyte. The redox couple is strongly coloured and competes with the dye for light absorption, particularly at lower wavelengths ( $\lambda_{max} I_3^- = 380 \text{ nm}$ , absorbs up to ca. 450 nm).<sup>14</sup> Additionally, the small energy difference between the redox potential of this electrolyte and the Fermi level of NiO limits the open-circuit voltage ( $V_{oc}$ ) of these devices. Great advances have been made recently, resulting in the implementation of Co, Fe and Cu-based inorganic redox couples and thiolate-based metal-free redox couples, which have led to a higher  $V_{oc}$ .

In 2015 Bach et al. reported the application of an optically transparent thiolate/disulfide electrolyte based on 5,50 -dithiobis(1-phenyl-1H-tetrazole) and sodium 1-phenyl-1H-tetrazole-5-thiolate as redox couple (Figure 35).<sup>120</sup> The redox potential of the thiolate electrolyte (245 mV vs. NHE) lies about 70 mV more negative than that of the iodide electrolyte (315 mV vs. NHE), offering an opportunity to improve the  $V_{oc}$  of p-DSCs. An improvement in  $V_{oc}$  of the p-DSCs containing the thiolate-based electrolyte compared to the devices containing iodide-based electrolyte was observed, while a similar  $J_{sc}$  (5.3  $\text{mA cm}^{-2}$ ) was maintained. In the same year, a device based on a commercially available and inexpensive coordination complex tris(acetylacetonato)iron(III)/(II) ( $[Fe(acac)_3]^{0/1-}$  (Figure 36) in conjunction with the PMI-6T-TPA sensitizer was reported. Solar cells made with the present electrolyte and incorporating a NiO blocking layer and chenodeoxycholic acid as an electrolyte additive produced PCE = 2.5%,<sup>45</sup> which was the highest reported efficiency for a p-type DSC at that time. The photovoltage was relatively low however, and this was attributed to fast charge recombination across the FTO/electrolyte interface, even in the presence of an NiO blocking layer.

**Figure 36.** Molecular structures of  $[Fe(acac)_3]^{0/1-}$ .<sup>45</sup>

**Figure 37.** Molecular structure of the cobalt complexes investigated as redox couples in p-DSCs.<sup>44,100</sup>

Cobalt (II/III) complexes have proved to be the most promising alternative to the  $I^-/I_3^-$  redox couple so far, due to the improved chemical stability of the device, better optical transparency and more negative redox potentials (vs.  $I^-/I_3^-$ ). Also, the size of these complexes can be tuned to reduce recombination between the redox electrolyte and holes in the NiO, as previously mentioned

in section 3.<sup>100</sup> Devices made using cobalt-based electrolytes typically produce a higher PCE than  $I^-/I_3^-$  (when comparing the same dye) due to a higher  $V_{oc}$  (ca. 200-300 mV vs. 100 mV).<sup>44</sup> However, not all dyes can be used with transition metal-based electrolytes, as a long-lived charge-separated state is necessary for dye regeneration to compete with charge recombination at the dye|NiO<sup>+</sup> interface. Most dyes used with these electrolytes contain a secondary electron acceptor, such as PMI or NDI, to generate long-lived radical species.<sup>44,100</sup> In 2009 an impressive  $V_{oc}$  of 0.35 V was obtained for the p-DSC using  $Co^{II/III}(dtb-bipy)_3^{2+/3+}$  as the electrolyte, giving a PCE of 0.2% (Figure 36).<sup>39</sup> Furthermore, in 2011, members of the same group reported a series of cobalt polypyridyl-based complexes with p-DSCs PCE ranging from 0.04 to 0.24% (Figure 37).<sup>100</sup> The most significant breakthrough so far has been the application of a novel electrolyte based on  $Co^{II/III}$  tris(1,2-diaminoethane) ( $[Co(en)_3]^{2+/3+}$ ) (Figure 37), which allowed p-DSCs to achieve a PCE = 1.3% with PMI-6T-TPA dye and NiO.<sup>44</sup>

In addition to metal complex-based electrolytes, polyoxometalates (POMs) are well-known anionic metal oxide clusters that have favourable electrochemical properties, are easy to prepare and are based on cheap starting materials.<sup>136</sup> Recent applications of POMs include water oxidation catalysts, as components in redox flow batteries, lithium ion batteries and super capacitors<sup>137-140</sup>. POMs have also been used as co-adsorbents on the surface of NiO electrodes in p-type DSCs and were shown to decrease the recombination rate and increase the  $V_{oc}$ .<sup>141</sup> Recently, POMs have been applied directly as redox mediators in p-DSCs by Reek et al.<sup>142</sup> Their study incorporated Lindqvist POMs which have a molecular formula  $M_6O_{19}^{2-}$  and a spherical shape, in the electrolyte solution. A unique feature of these POMs as electrolytes is that they are transparent and can therefore be suitable for tandem solar cell applications. Furthermore, they found give a 4 to 5-fold increase in  $V_{oc}$  when applying these POM electrolytes in comparison to the devices with the traditional  $I_3^-/I^-$  couple. Currently, the low solubility of the POMs is the main limiting factor for increasing the short-circuit current of these cells. Increasing the solubility of these POM materials should therefore be the main focus point when improving the efficiency of these cells.

The same optimization approach was applied to other semiconductors, including CuO (see section 5).<sup>151</sup> Guldi and co-workers found acetonitrile to be the most suitable solvent for CuO p-DSCs, which is consistent with NiO devices. The 4-*tert*-butyl-pyridine (4-tbp) and  $Li^+$  addition was also screened. In general, 4-tbp exerted no notable impact on the PCE, as previously demonstrated for NiO by Hagfeldt *et al.*<sup>20</sup> There was, however, a significant concentration dependence observed for  $Li^+$ : the authors proposed that the  $Li^+$  affects the distribution of trap states, which, in turn, suppresses the recombination with the electrolyte. It was suggested that at high  $Li^+$  concentrations, the formation of additional trap states in the valence band of CuO open new pathways for recombination through  $I^-$  adsorption on the electrode surface. An optimum  $Li^+$  concentration of 0.2 M was found for CuO-based p-DSCs, to balance charge injection, charge transport, and charge recombination. These optimum conditions resulted in device

efficiencies of up to 0.16%. The impact of three different ionic liquids on the electrolyte properties and device performance was also probed. EMII and DMPII showed superior diffusion and recombination properties, respectively, when compared to 1-butyl-3-methylimidazolium iodide (BMII), which has been used as iodine source before.<sup>151</sup>

The efficiencies of p-type DSCs with NiO and  $I_3^-/I^-$  as the redox couple has probably approached its optimum performance and further breakthroughs will require alternative electrolytes. The challenge is balancing the kinetic properties of the dye and redox mediator, i.e. a redox couple which is advantageous in terms of slow recombination with the NiO substrate may also be slow at regenerating the dye, and so more effort is required to prevent recombination at the dye-NiO interface. Organometallic systems are versatile in terms being able to functionalise the ligands to both tune the redox potential and the steric properties to balance fast diffusion but limiting the interaction with the NiO. New concepts are also emerging, such as POM-based redox shuttles, which can store charge, and solid-state charge-transport layers, which have obvious benefits for scale-up and stability. A dual shuttle approach, which is characterized by the use of a redox mediator in conjunction with a co-mediator, initially employed by Bignozzi *et al.*<sup>143</sup> for n-type dye sensitized solar cells, could also be employed in p-type devices to favour charge separation over recombination.

## 5. Semiconductors

The fabrication of sensitizers which permit a long-lived charge separated state at the dye|semiconductor interface is imperative to reduce parasitic charge recombination. Furthermore, their coupling with new electron mediators can dramatically improve device efficiencies. At the same time, several approaches have been employed to enhance the electronic characteristics of NiO or to find better performing semiconductors based on binary or ternary oxides, such as delafossites or spinel structures.

### 5.1 NiO

As previously mentioned, NiO is the most widely researched p-type semiconductor (SC), with a valence band edge at 0.3 V vs. SCE at pH 7 and a band gap of 3.6-4.0 eV.<sup>122</sup> NiO is essentially transparent at low thicknesses, although some brown colour is present due to intrinsic Ni(III) ions that form during sintering. Ni(III) is present as a result of Ni(II) vacancies in the material, and their presence is thought to be responsible for the p-type character of NiO, which otherwise would be a Mott insulator. Various techniques are used to prepare NiO films<sup>123,124</sup> including sol-gel, rapid discharge sintering (RDS), hydrothermal and screen-printing methods.<sup>23,123-127</sup> The most commonly used technique is the sol-gel method, due to its simplicity and reproducibility. A successful method for preparing mesoporous NiO films, which increases the surface area for dye adsorption, is to use triblock copolymers as templates in the sol-gel route. The method described by Sumikura *et al.*<sup>125</sup> is used to prepare F108-templated NiO films with thicknesses of 1-2  $\mu m$  and crystal sizes of 16 nm (after sintering at 450 °C). In this respect,

Gibson et al. investigated a range of different mesoporous NiO electrodes prepared by different research groups and private firms in Europe to determine the parameters which influence good quality photoelectrochemical devices. From these studies it appears that a crystallite size of at least 20 nm, a film thickness of 1–2  $\mu\text{m}$  and a specific surface area above 40  $\text{m}^2 \text{g}^{-1}$  is most appropriate for photoelectrochemical devices using NiO. In addition, for thinner films, a lower sintering temperature (350  $^\circ\text{C}$ ) gave better results than a higher sintering temperature (450  $^\circ\text{C}$  and 500  $^\circ\text{C}$ ).<sup>147</sup>

In addition to the conventional methods already employed to prepare NiO thin films, such as screen printing, spin coating and spray pyrolysis, many other methods have been employed.<sup>144</sup> One example of preparing metal oxides with high specific surface area is electrospinning, which is simple, controllable, versatile and cost-effective approach. This method has been employed in the synthesis of NiO electrodes for supercapacitors, otherwise it can be easily shifted to semiconductor preparation for p-type dye sensitized solar cells. Electrospun metal oxide nanofibers are characterized by granular and fibrous morphology, high aspect ratio and large surface to volume ratio, high crystallinity and improved mechanical strength, which makes them potentially ideal candidate for solar cells.<sup>145</sup> Furthermore, Jousseme et al. reported the synthesis of mesoporous NiO films through inkjet printing of a sol-gel ink for the first time. Multilayer NiO films were formed, and different morphologies could be obtained by playing on the interlayer thermal treatment. The different morphologies and thicknesses of the NiO films were correlated to their performance in a p-DSC configuration, using a push-pull dye and an iodine-based electrolyte. The best results were obtained with NiOx/four layer-NiO mesoporous photocathodes of 860 nm, with a current density at the short circuit of 3.42  $\text{mA cm}^{-2}$ .<sup>146</sup>

Although its broad usage, NiO is not free from issues. For example, NiO has a low hole mobility ( $10^{-8} - 0.141 \text{ cm}^2 \text{V}^{-1} \text{s}^{-1}$ ), as discussed in section 3.<sup>130</sup> This leads to a small diffusion length for holes (2-3  $\mu\text{m}$ ), which is not observed in  $\text{TiO}_2$  where the electron diffusion coefficient is two orders of magnitude faster. The PV performance of NiO p-DSCs has been hampered as a consequence of the poor conductivity of the electrodes, which leads to fast charge recombination (CR) and poor injection yield ( $n_{inj}$ ), depleting the number of collected charges and PCE.<sup>128</sup> Charge recombination at the dye|NiO interface has been seen to occur in the Marcus normal region, in which recombination increases with increasing driving force.<sup>128</sup> Several strategies have been employed to improve the performance of p-DSCs with NiO electrodes. For example, Hammarström and co-workers found that surface  $\text{Ni}^{3+}$  states were involved in hole trapping.<sup>130</sup> These states act as tunnelling sites that rapidly trap holes on a sub-ps timescale, forming high energy  $\text{Ni}_{(h)}^{4+}$  states, that recombine with the reduced dye/redox mediator rapidly (100 ns). The authors proposed that reducing the reactivity of the  $\text{Ni}_{(h)}^{4+}$  hole would improve the device performance. For example, removing the  $\text{Ni}^{3+}$  sites from the surface of NiO by chemical reduction would avoid “ $\text{Ni}^{4+}$ ” formation, or retarding the electron recombination with  $\text{Ni}_{(h)}^{4+}$  to lifetimes longer than

100–200 ns would, instead, allow the relaxation to the  $\text{Ni}_{(h)}^{3+}$  hole, for which recombination is much slower. The authors subsequently showed that the reduction of high valence Ni impurities,  $\text{Ni}^{3+}$  and  $\text{Ni}^{4+}$  to  $\text{Ni}^{2+}$ , at the electrode surface by both chemical and thermal methods, decreased the charge recombination with the electrolyte.<sup>85</sup> The chemical method, which involved immersing the NiO electrodes in an acetonitrile solution of a hydride source,  $\text{NaBH}_4$ , before sensitization with the dye, was successful in reducing NiO high valence states. The thermal treatment of NiO at 200 $^\circ\text{C}$  led to the decomposition of  $\text{Ni}^{\text{III}}\text{OOH}$  impurities to NiO, oxygen, and water. The group proposed that this heat treatment affected the dye adsorption and trap state distribution, which contributed to preventing recombination and lowering the quasi Fermi level, which manifested in an increase in the  $V_{oc}$  compared the untreated films.

Wu and co-workers reduced the rapid charge recombination between the photoreduced dye and the injected hole into the NiO semiconductor, by means of modifying the photocathode with an aqueous nickel salt.<sup>131</sup> As a result, a denser and highly crystalline nanostructure was acquired on the NiO electrode, which led to an increase in the current density and photovoltage compared with the untreated NiO film. The authors attributed the improvement to a shift in the Fermi level due to a change in the stoichiometry of the nickel and oxygen atoms on the surface of the modified electrode, resulting in an increase of the  $V_{oc}$  and a 35.7 % increase in the PCE of the p-DSC.

Blocking layers have also been employed to improve performance, being well-known to reduce recombination with FTO. A number of approaches have been taken to apply a thin compact layer of NiO on the FTO substrate, for example by spray pyrolysis of a precursor solution of  $[\text{Ni}(\text{acac})_2]$ , which has been observed to improve the PCE.<sup>132</sup> Wu et al. found that applying an alumina coating as a blocking layer in NiO based p-type DSCs could enhance the PCE by 74%, while atomic deposition of boron or spraying a  $\text{TiO}_2$  compact layer onto the NiO film produced a similar effect of suppressing the recombination, as discussed in section 3.<sup>110,111</sup>

Odobel *et al.* proposed another strategy, filling the gaps in the dye monolayer with an insulating, transparent, bulky organic molecule, namely chenodeoxycholic acid (CDCA), which has been used widely in  $\text{TiO}_2$  DSCs to avoid aggregation of the dye, according to two methods; either directly dissolving CDCA in the electrolyte (where the dye was sufficiently insoluble in the electrolyte solvent to avoid leaching) or, when CDCA was poorly soluble in the electrolyte solvent, by depositing CDCA directly on the photocathode by spin coating.<sup>113</sup> In both methods the authors found that the vacant sites were efficiently covered by CDCA molecules, reducing the charge-recombination at the electrode surface (see section 3), but without competition with the photosensitizer for adsorption sites, thus leaving the light harvesting efficiency of the electrode unaffected. Interestingly, the  $V_{oc}$  increased by 25% when CDCA was dissolved in iodine-based electrolyte, and an impressive 65% rise was recorded when CDCA was spin coated onto the photocathode, reaching 540 mV on NiO in the presence of a cobalt-based electrolyte. This strategy seems to be generally applicable as it was

successful with different benchmark dyes such as P1 and DPP-NDI.

The doping of NiO with atomic impurities has shown promising effects on the performance of p-DSCs. NiO was successfully doped with Co, Mg and, in particular, Li. Wu and co-workers systematically prepared nanoparticulate films composed of solid solutions of NiO with 2, 6 and 10% cobalt.<sup>98</sup> Their electrochemical study on doping effect is reported in section 4. The authors found that the density of acceptor states around the valence band edge of NiO nanoparticles increased and the Fermi energy level was lowered gradually upon addition of cobalt. Consequently, the  $V_{oc}$  increased with increasing concentration of cobalt and the maximum increase was obtained for the nominally 6% wt. Co-film. Adding Mg to the NiO photocathode also enhanced the open-circuit voltage, however, this was offset with a decrease in the photocurrent with increasing  $Mg^{2+}$  content.<sup>134</sup> The cause of this has been attributed to a positive shift in the energy of the valence band, which decreased the driving force for electron transfer from the NiO film to the dye. A MgO doping concentration of 5% wt. was found to strike a balance between increasing  $V_{oc}$  and decreasing  $J_{sc}$ , which lead to an optimum PCE. Chen *et al.* improved the PCE of p-DSCs by about 85% for electrodes based on a solid solution of Mg-NiO compared to pure NiO.<sup>133</sup>

Li doping of NiO, where  $Ni^{2+}$  is substituted with  $Li^+$ , creates an electron vacancy, increasing the number of charge carriers (holes) and leading to a shift in the valence band edge. Li doping of NiO has been extensively studied over several decades for applications in capacitors and batteries.<sup>135</sup> p-Type DSCs containing Li-doped NiO also suffered from declining hole injection efficiency, but this has been offset with a decrease in hole recombination, and improved hole transport, which resulted in enhanced collection efficiency and photovoltaic performance.<sup>116</sup>

In addition to doping, the preparation of NiO composites have also been considered: in particular, graphene/NiO thin-film composites have shown a suppression in charge recombination, ascribed to the presence of graphene enhancing hole transport thus achieving efficient electron-hole pair separation and collection.<sup>148</sup> Despite improvements, NiO presents intrinsic limitations which are challenging to overcome. One of the most compelling motivators for alternative p-TCOs is that the VB of NiO (0.54 V vs NHE) is very close to redox potential of most of the electrolytes. To match the built-in potential of  $TiO_2$  devices, the VB of the p-type semiconductor needs to be about 0.5 V more positive than NiO.

## 5.2 Binary oxides

**Figure 38.** Molecular structure of dye examined by Suzuki *et al.* in conjunction with CuO.

Among the alternative p-type binary oxides which have been studied, cupric oxide (CuO) has gathered much attention in numerous applications including solar cells, due to its ease of fabrication with high chemical and thermal stability and tuneable electronic properties.<sup>149</sup> CuO films have a deeper

valence band compared to NiO, as shown in Table 2, and a higher dielectric constant with respect to NiO ( $CuO \epsilon = 18.1$  vs.  $NiO \epsilon = 9.7$ ).<sup>19,149</sup> Consequently, the likelihood of electron-hole dissociation should be higher, increasing the charge collection efficiency. Suzuki *et al.* were the first to report a DSC based on CuO, which was sensitized with Fast Green FCF and NK-3628 (Figure 38), and the corresponding devices generated a PCE of approximately 0.01%.<sup>149</sup>

**Figure 39.** Molecular structure of electron-accepting dyes ZnPc1, ZnPc3 and ZnPc4 investigated in conjunction with CuO.<sup>154</sup> The dyes feature phenyl-ethynyl (ZnPc3) and triphenylamine-ethynyl (ZnPc4) spacers, to control the charge recombination between the CuO photocathode and the reduced ZnPc, and implement a "push-pull" design in the case of ZnPc4.

More recently, Guldi and co-workers reported a p-DSC based on nanorod-like CuO electrodes, employing zinc phthalocyanines (ZnPc1 and ZnPc2) as sensitizers (Figure 39). They obtained respectable PCEs of 0.103% and 0.191% with iodide and cobalt redox mediators respectively.<sup>150</sup> The group have characterised the impact of CuO electrode fabrication, calcination temperature and electrode thickness, and the  $I^-/I_3^-$  electrolyte ratio on the device performance by combining device analysis and electrochemical impedance spectroscopy (EIS), as described in section 3.<sup>114</sup> Guldi *et al.* found that nanoparticles prepared by the precipitation of CuO via  $Cu(OH)_2$  were superior (PCE = 0.11%) to commercial CuO nanoparticles (PCE = 0.073%).<sup>151</sup> The authors attributed the improved performance to the smaller size of the precipitated nanoparticles which had a higher specific surface area and a higher uptake of the photosensitizer compared to the commercial material. Furthermore the corresponding devices showed an improved charge injection and charge-transport lifetime and, consequently a higher  $J_{sc}$  ( $3.4 \text{ mAcm}^{-2}$ ).<sup>152</sup> Guldi *et al.* assembled a t-DSC incorporating the optimised electrodes, sensitized with electron-accepting ZnPcs (Figure 39).<sup>153</sup> ZnPc3 and ZnPc4 performed better in terms of  $V_{oc}$  and FF than the previously reported ZnPc1, which the authors attribute to higher dye loadings and a more efficient charge separation/hindered charge recombination. However, the  $J_{sc}$  was moderate ( $1.17 \text{ mAcm}^{-2}$  for ZnPc4 and  $1.57 \text{ mAcm}^{-2}$  for ZnPc3), due to limited charge injection. The low-energy absorptions of ZnPcs are potentially useful for tandem cells, however, and the t-DSCs assembled with ZnPc4 gave the best PCE of 0.69%.

Obodel *et al.* tested CuO nanowires and nanorods sensitized with P1 and two DPP based derivatives (DPP-NDI and YF1) in p-DSCs.<sup>154</sup> The researchers found that cobalt redox mediators were more suitable for CuO electrodes, which were found to be unstable towards  $I^-/I_3^-$ . In this study, the reported average transport time in CuO was shorter than in NiO, which the authors propose could be due to a higher conductivity for CuO, arising from the wire-like morphology. Finally, the intrinsic absorbance of CuO competed with light absorption of the sensitizers and offers a pathway to quench the dye excited state by energy transfer. Despite this, it was noted that dyes featuring a high molar extinction coefficient and an absorption profile around 600 nm gave promising results. It is therefore possible

that CuO could represent a viable cathode material for solar cells provided that it is sensitized with a dye harvesting low energy photons such as those above 700 nm. For example, this is feasible in t-DSCs where the photoanode could capture most of the visible photons and transmit the lower energy region of the solar spectrum to be collected by the photocathode.

Cuprous oxide (Cu<sub>2</sub>O) is also a potentially interesting p-type semiconductor, however, the electrode made of only Cu<sub>2</sub>O has rarely been investigated, probably due to the natural instability of Cu<sub>2</sub>O in the presence of an electrolyte.<sup>155</sup> Lu *et al.* presented a simple method for the preparation of Cu<sub>2</sub>O films for DSCs, obtaining an open-circuit voltage of 0.71 V, a short-circuit current density of 1.3 mA cm<sup>-2</sup>, a fill factor of 46%, and a PCE of 0.42% with the C343 dye.<sup>156</sup> Following this interesting result, Cu<sub>2</sub>O was used in core-shell structures with CuO.<sup>157</sup> Cu<sub>2</sub>O@CuO core-shell nanoparticles were synthesized via a facile precipitation-thermal oxidation method consisting of the preparation of Cu<sub>2</sub>O nanoparticles in solution followed by a post-treatment at 300 °C, 350 °C or 400 °C in air. This shell may be viewed as a passivating layer that overcomes the natural chemical instability of Cu<sub>2</sub>O towards electrolytes. Furthermore, the energy barrier formed at the interface between the core and shell facilitates the transfer of the holes from the CuO to the Cu<sub>2</sub>O to enhance the injection efficiency of the excited dye. The Cu<sub>2</sub>O@CuO based p-DSC gave a V<sub>oc</sub> = 315 mV and a J<sub>sc</sub> = 0.14 mA cm<sup>-2</sup>. The J<sub>sc</sub> value remains unsatisfactory and consequently leads to the relatively low PCE = 0.017%, due to the low specific surface area of Cu<sub>2</sub>O@CuO compared with other materials and the competition for light absorption between DPP-NDI and both CuO and Cu<sub>2</sub>O themselves. In addition to choosing photosensitizers which absorb > 600 nm, the authors suggest that decreasing the size of the Cu<sub>2</sub>O@CuO core-shell nanoparticles or preparing the Cu<sub>2</sub>O@CuO core-shell materials with hierarchical structure to increase the specific surface area for favourable dye loading should improve the performance.

Other binary oxides, such as ZnO and ITO have also been applied in dye-sensitized photocathodes. ZnO nanostructures have been widely studied across a broad range of optical and electronic applications. ZnO nanostructures typically show n-type conductivity and can be prepared by vapor process, vapor-liquid-solid growth method, or grown via surface reaction of organic or metal-organic precursor compounds.<sup>160</sup> Group III elements such as Al, Ga, and In are commonly added as extrinsic dopants. However, Gupta *et al.* showed that the dopant K has a strong influence on the carrier density and mobility of p-type ZnO.<sup>158</sup> Wang and co-workers examined the effect of K as a dopant in transparent, nanocrystalline ZnO and successfully produced a p-type semiconductor for p-DSC applications.<sup>159</sup> The K-doped ZnO thin-films showed high optical transparency (>85%) and reasonable hole diffusion (10<sup>-6</sup> cm<sup>2</sup> s<sup>-1</sup>), which were comparable to NiO, making them viable for p-DSCs.<sup>159</sup> The films were sensitized with C343 and applied in p-DSCs, which gave almost promising J<sub>sc</sub> (0.408 mA cm<sup>-2</sup>), V<sub>oc</sub> (82 mV), and PCE (0.0012%). The authors reported that the charge recombination with electrolyte in solution was lower compared to that observed in NiO-based devices and proposed that alternative

sensitizers with optimised alignment of the HOMO level with the ZnO valence band would improve the results, however, to our knowledge, no further studies have yet been reported. Indeed, in the present case, the flat-band potential for the K-doped ZnO (being related to the doping level) indicates that the valence band of the semiconductor might not be suitable for hole injection for p-DSC applications, due to a large potential offset (about +0.2 eV) related to the HOMO energy level (5.9 eV vs. vacuum) of the C343 sensitizer employed in the work.

Tin-doped indium oxide (ITO) is a degenerate n-SC with a bandgap around 3.7–3.8 eV. However, it has been shown to be able to accept or donate electrons from photosensitizers. Huang *et al.* first reported that p-DSCs can be constructed onto mesoporous ITO films coated with a ruthenium-dye.<sup>161</sup> Although high photocurrents were achieved of up to 5.96 mA cm<sup>-2</sup>, which are close to the highest recorded in conventional p-type sensitized photocathodes, the PCE was limited by the low V<sub>oc</sub> that were achieved with the I<sub>3</sub><sup>-</sup>/I<sup>-</sup>-based electrolyte. Bach and co-workers replaced the I<sub>3</sub><sup>-</sup>/I<sup>-</sup> with [Fe(acac)<sub>3</sub>]<sup>0/-</sup> in p-DSCs based on ITO films bearing the organic dye, PMI-8T-TPA, which is optimised for photocathodes.<sup>162</sup> PCEs of ca. 2% were achieved using this strategy which rival the best reported PCE of 2.5% for analogous devices based on NiO. Work on binary oxides so far has highlighted a key problem in the trade-off between good conductivity and high transparency. This is particularly apparent with CuO, which, despite higher V<sub>oc</sub> obtained, the absorptivity of the electrode was too high in the visible region, leading to competition with the dye for light absorption and, accordingly, limiting DSC performance. At the same time, the instability of Cu<sub>2</sub>O has limited its application and this is a well-known issue also for p-type ZnO. Further studies are required to exploit the favourable properties of K-doped ZnO in p-type DSCs, such as screening with different combinations of electrolytes and dyes. Since charge recombination is reported to be slower with these semiconductors, they could be potentially be coupled with a faster redox couple, such as iron acetylacetonate. However, until now, the best result with a binary oxide alternative to NiO, was obtained with ITO in conjunction with a dye with a donor acceptor structure. However, at the moment, the behaviour is comparable with, but not superior to, the best performing DSC made with NiO.

### 5.3 Ternary and quaternary oxides

An alternative solution to poor hole mobility is to fabricate TCOs which have an element with full 3d orbitals close in energy to the oxygen 2p orbitals, so that hybridisation would delocalise this state and reduce the hole effective mass. One proposed way of achieving this is to use delafossite-structured Cu(I) ternary oxides. The Cu<sup>I</sup>-based delafossite structure, Cu<sup>I</sup>M<sup>III</sup>O<sub>2</sub>, can accommodate a wide range of rare earth and transition metal cations on the M<sup>III</sup> site. Substitutional doping of divalent ions for these trivalent metals is known to produce higher p-type conductivity than is observed in the corresponding undoped materials. This class of p-type TCOs were proposed in 1997 by Hosono and co-workers, who first reported the optical and electrical properties of copper aluminate (CuAlO<sub>2</sub>), which

crystallizes in the delafossite structure.<sup>163</sup> This sparked an explosion of interest in developing p-type TCOs using Hosono's approach "chemical modulation of the valence band" to combine the p-type conductivity of Cu<sub>2</sub>O with the larger band gaps of other binary oxides. Ternary Cu-based delafossite materials retain the valence band features of Cu<sub>2</sub>O, with the Cu states dominating the top of the valence band, while extending the band gap by alloying with the wide band gap trivalent binary oxide. In the delafossite structure, each Cu atom is linearly coordinated with two oxygen atoms, forming O–Cu–O dumbbells parallel to the *c* axis (Figure 40). Oxygens in these O–Cu–O units are also each coordinated to three M<sup>III</sup> atoms, which are oriented such that M<sup>III</sup>-centred octahedra form M<sup>III</sup>O<sub>2</sub> layers that lie parallel to the *ab* plane. Two alternative layer stackings are possible, resulting in a hexagonal (space group *P63/mmc*) or rhombohedral (space group *R3-mh*) unit cell.<sup>164</sup>

**Figure 40.** The hexagonal delafossite structure. The green, red, and blue spheres are M<sup>III</sup>, oxygen, and copper, respectively.<sup>164</sup>

The prototypical copper delafossite TCO, CuAlO<sub>2</sub>, has received most of the attention. The delafossite structure of CuAlO<sub>2</sub> is comprised of alternating layers of slightly distorted edge-shared AlO<sub>6</sub> octahedra and two-dimensional close-packed Cu<sup>1+</sup> cations. Depending on the stacking of the layers, two polytypes are possible. The "3R" polytype consists of "AaBbCcAaBbCc..." stacking along the *c*-axis and has rhombohedral symmetry with the space group *R-3m*, whereas the "2H" polytype consists of an alternate stacking sequence ("AaB-bAaBb...") and has the space group *P63/mmc*.<sup>163</sup> The suitability of a CuAlO<sub>2</sub> as a hole conductor was first demonstrated in a solid-state DSC by Yasomanee and co-workers.<sup>165</sup> Later, Cheng and co-workers produced CuAlO<sub>2</sub> photocathodes by a solid-state reaction observing particle sizes of 1-2 μm.<sup>166</sup> The photocathodes were then sensitized with PMI-6T-TPA for assembly in p-DSCs. The driving force for hole injection was found to be sufficient, however, the large particle size, low dye loading and low specific surface area (1.7 m<sup>2</sup> g<sup>-1</sup>) resulted in low J<sub>sc</sub> (0.3 mA cm<sup>-2</sup>). In addition, a relatively large V<sub>oc</sub> (333 mV) was recorded compared to analogous I<sup>-</sup>/I<sub>3</sub><sup>-</sup> and NiO-based DSCs. Enhancements in the J<sub>sc</sub> (0.954 mA cm<sup>-2</sup>) were then reported by applying a solid-state synthesis, under controlled partial oxygen pressures of 10<sup>-5</sup> atm at 775°C, which gave pure phase CuAlO<sub>2</sub> nanoparticles (diameter = 35 nm). Despite a higher J<sub>sc</sub>, the overall PCE (0.037%) was still lower than previously reports.<sup>167</sup> Recently, a study focusing on the effect of polymorphism on PV performance found that even in small concentration the presence of the 2H polytype of CuAlO<sub>2</sub> lead to a 49% increase in the PCE compared to the pure 3R-CuAlO<sub>2</sub> polytype.<sup>168</sup> In the delafossite CuMO<sub>2</sub> materials, the optically measured direct bandgap increases from M = Al, Ga to In, and CuGaO<sub>2</sub> should exhibit better transparency than CuAlO<sub>2</sub>. Furthermore, the VB edge of CuGaO<sub>2</sub> is about 5.3 eV below vacuum level, which is lower than that of NiO. CuGaO<sub>2</sub>-based p-DSCs should thus generate higher photovoltages than NiO. CuGaO<sub>2</sub> based photocathodes were sensitized with P1 and assembled in p-

DSCs which, indeed, increased the V<sub>oc</sub> compared to NiO (I<sup>-</sup>/I<sub>3</sub><sup>-</sup>: CuGaO<sub>2</sub> = 234 mV vs NiO = 132 mV). However, the limiting parameter was the J<sub>sc</sub> (0.4 mA cm<sup>-2</sup>), which the authors attributed to the lower specific surface area of their CuGaO<sub>2</sub> electrodes (CuGaO<sub>2</sub> = 30 m<sup>2</sup> g<sup>-1</sup> vs NiO = 158 m<sup>2</sup> g<sup>-1</sup>), which limited the PCE (0.026%). Generally, the main challenge with this class of materials is the difficulty in synthesizing the delafossite CuMO<sub>2</sub> nanoparticles. Wu and co-workers reported CuGaO<sub>2</sub> nanoplates produced by a hydrothermal synthesis route, which is known to be promising to achieve small particle dimensions.<sup>169</sup> Much higher J<sub>sc</sub> (2.05 mA cm<sup>-2</sup>) was reported for thin-films made of small nanoplates (25 nm in average thickness, 100–200 nm in average diameter) prepared by a hydrothermal synthesis of CuGaO<sub>2</sub>.<sup>172</sup> When the benchmark P1 dye and an I<sup>-</sup>/I<sub>3</sub><sup>-</sup> electrolyte were combined with the optimal CuGaO<sub>2</sub> photocathode, a PCE of 0.18% was attained.

Attempts to increase the J<sub>sc</sub> include doping or alloying with other cations, for example, Mg-doped CuGaO<sub>2</sub> has been synthesized with small concentrations of Mg added: the photocathodes provided a higher specific surface area and higher PCE with respect to the bare CuGaO<sub>2</sub> (0.045% for Mg doped CuGaO<sub>2</sub>).<sup>170</sup> Indeed, Jobic *et al.* reported nanostructured CuGaO<sub>2</sub> and its Mg doped derivatives synthesised via hydrothermal conditions.<sup>170</sup> Their results indicate that a low amount of magnesium helps in preparing samples with higher specific surface areas and increasing the PCE. The corresponding p-DSCs assembled with the PMI-NDI dyad and a tris(4,4'-bis-tert-butyl-2,2'-bipyridine) cobalt(II/III)-based electrolyte attained conversion efficiencies similar to those typically reported for NiO. Fe-doped CuGaO<sub>2</sub> has also been applied in p-DSCs and improvements were observed in the dye loading, the overall conductivity and the PV performance.<sup>171</sup> Al-doped CuGaO<sub>2</sub> has also been synthesized employing the hydrothermal method and its properties have been investigated as a cathode with ruthenium dye N719. The J<sub>sc</sub> and V<sub>oc</sub> for 5% Al-doped CuGaO<sub>2</sub> microparticles coated with N719 dye were two times higher than undoped CuGaO<sub>2</sub> microparticles.<sup>173</sup> CuFeO<sub>2</sub>, CuBO<sub>2</sub>, and CuCrO<sub>2</sub> photocathodes have also been reported.<sup>176</sup> CuCrO<sub>2</sub> has so far been the most promising Cu-based delafossite for p-type devices and has also attracted attention for a range of applications beyond TCOs. In the condensed matter physics community, CuCrO<sub>2</sub> has been investigated for its unusual magnetic properties due to its frustrated antiferromagnetic ordering and multiferroic properties.<sup>174</sup> The higher conductivities of CuCrO<sub>2</sub> compared to other delafossites is attributed to favourable mixing of Cr *d* states with O 2p states in the valence band producing shallower transition levels for the Cu-based holes. Furthermore, the top of the valence band is found to be dominated by the Cu *d* states and both theory and experimental data are consistent with conductivity through the Cu(I)/Cu(II) hole-transport mechanism.<sup>174,175</sup>

In 2012, Chen and co-workers reported a hydrothermal method to synthesise delafossite CuCrO<sub>2</sub> nanocrystals (ca. 20 nm) and applied them as photocathodes in p-type DSCs for the first time.<sup>176</sup> Under optimized conditions, a V<sub>oc</sub> of 102 mV, a J<sub>sc</sub> of 0.491 mA cm<sup>2</sup>, a fill factor of 0.398 and an overall PCE of 0.019%

were finally achieved for a C343 dye sensitized  $\text{CuCrO}_2$  solar cell. These values were comparable with a DSC based on a NiO photocathode prepared and tested in similar experimental conditions.

To improve the device performance, different sensitizers and electron mediators have been tested. For example, Bach *et al.* sensitized screen-printed thin mesoporous electrodes of  $\text{CuCrO}_2$  nanoparticles, prepared by a hydrothermal route, with PMI-6T-TPA and applied the photocathodes in p-DSCs with the  $[\text{Co}(\text{en})_3]^{2+/3+}$  electrolyte.<sup>177</sup> Compared to the equivalent device with NiO, the  $V_{\text{OC}}$  was higher, reaching 734 mV, which was attributed to a slightly lower valence band edge of  $\text{CuCrO}_2$  with respect to NiO. Furthermore, the improved  $V_{\text{OC}}$  could be due to a reduced charge recombination with  $\text{CuCrO}_2$ . Indeed, the observed transient lifetime in  $\text{CuCrO}_2$  ( $140 \pm 15 \mu\text{s}$ ) and NiO DSCs ( $24 \pm 0.4 \mu\text{s}$ ) indicate an overall reduced recombination rate for  $\text{CuCrO}_2$ . Unfortunately, this  $V_{\text{OC}}$  increase was offset by a significant decrease in photocurrent ( $3.74 \text{ mA cm}^{-2}$  for NiO with respect to  $1.23 \text{ mA cm}^{-2}$  for  $\text{CuCrO}_2$ ).<sup>177</sup> The authors concluded that the cause of the drop in photocurrent was insufficient driving force for the hole-injection, rather than any intrinsic material properties of  $\text{CuCrO}_2$ . The driving forces for hole injection from PMI-6T-TPA\* into the valence bands of  $\text{CuCrO}_2$  and NiO are  $\sim 0.3$  and  $\sim 0.4$  eV respectively. Mori *et al.* recently reported that hole-injection rates scaled with driving forces up to  $\Delta E$  values of 0.6 eV, thus providing a strong indication that insufficient hole injection driving forces are hampering the performance of PMI-6T-TPA-sensitized  $\text{CuCrO}_2$  p-DSCs.<sup>28,178</sup>

This suggests that the latest generation of high performance, p-type sensitizers could be inadequate for the sensitization of alternative p-type semiconductors where there is a ca. 100 mV drop in the energy of the valence band edge, compared to NiO. In the future, it may be necessary to tailor sensitizers to match the electronic properties of the new materials in order to fully exploit their potential.

Chen *et al.* attempted to increase the photocurrent generated by  $\text{CuCrO}_2$ , sensitized with P1, by adding Au nanoparticles to augment the light absorption from the dye. The authors assembled the photocathodes in p-DSCs with a disulfide/thiolate redox shuttle, which attained a PCE of 0.31%. The near field induced by Au NPs improved the photocurrent, reaching a value around  $3 \text{ mA cm}^{-2}$  with respect to  $1.5 \text{ mA cm}^{-2}$  obtained without Au nanoparticles, without affecting the interfacial recombination kinetic dynamics or the electronic energy levels of the semiconductor.<sup>179</sup>

Other attempts to improve the photocurrent of  $\text{CuCrO}_2$  devices include doping the material to improve the conductivity. It was found that Mg-doped  $\text{CuCrO}_2$  films (with 10% Mg) attain a conductivity greater than many other p-type TCO ( $\sim 220 \text{ S cm}^{-1}$ ). Chen *et al.* applied Mg-doped  $\text{CuCrO}_2$  nanocrystals, prepared by hydrothermal synthesis, in p-type DSCs, with P1 and iodine-based electrolyte. Generally, ultrasmall size is the biggest advantage of  $\text{CuCrO}_2$  and  $\text{CuCr}_{0.9}\text{Mg}_{0.1}\text{O}_2$  nanocrystals introduced by the authors show small dimension particles almost over any other reported delafossite oxides applied in the p-type DSC systems (ca. 40 nm and ca. 50 nm respectively). A PCE improvement of approximately 30% was achieved through

adding Mg, mainly due to an increase in  $J_{\text{SC}}$  (by 27%).<sup>180</sup> The increase in  $J_{\text{SC}}$  for the doped films was attributed to a larger surface area ( $23 \text{ m}^2 \text{ g}^{-1}$  for  $\text{CuCrO}_2$  and  $15 \text{ m}^2 \text{ g}^{-1}$  for  $\text{CuCr}_{0.9}\text{Mg}_{0.1}\text{O}_2$ ) and higher light harvesting efficiency. The  $V_{\text{OC}}$ ,  $J_{\text{SC}}$ , and PCE of the optimal  $\text{CuCr}_{0.9}\text{Mg}_{0.1}\text{O}_2$ -based DSC device were 201 mV,  $1.51 \text{ mA cm}^{-2}$  and 0.13%, respectively, being higher than that for the equivalent NiO reference when tested under the same conditions.  $\text{CuCrO}_2$  has also been doped with different species such as Ga and Co.<sup>181,182</sup> The specific hydrothermal conditions (temperature, pressure and molarity of basic solution) determine the concentration of excess oxygen in the delafossite material and by Co-substitution for Cr the observed electrical resistivity further decreases in the non-stoichiometric nanocrystals.<sup>181</sup> P-DSCs assembled with Co-doped  $\text{CuCrO}_2$  using two types of dye, C343 and N719 and  $\text{I}^-/\text{I}_3^-$  as the redox couple, gave PCEs of around 0.01%. The  $J_{\text{SC}}$  was higher by approximately 40% when N719 was used as dye compared to C343 ( $0.5 \text{ mA cm}^{-2}$  and  $0.3 \text{ mA cm}^{-2}$  respectively). Partial substitution of Cr for Ga has provided more encouraging results.<sup>182</sup> The difference between the ionic radius of Cr (0.52 Å) and Ga (0.62 Å) is sufficiently small that solid solutions of  $\text{CuCr}_{1-x}\text{Ga}_x\text{O}_2$  from  $0 < x < 1$  can be prepared. Pure phase nanocrystals of  $\text{CuCr}_{1-x}\text{Ga}_x\text{O}_2$  with the crystal sizes ranging from 15 nm to 50 nm, prepared by hydrothermal synthesis, were reported by Chen *et al.*<sup>182</sup> The corresponding p-DSCs attained optimum values of  $V_{\text{OC}} = 134 \text{ mV}$ ,  $J_{\text{SC}} = 1.56 \text{ mA cm}^{-2}$  and PCE = 0.10%, which was comparable to that of  $\text{CuCrO}_2$  reported in the same paper.

The reported conductivity of  $\text{CuFeO}_2$  is relatively higher compared to other delafossites, excluding  $\text{CuCrO}_2$ .<sup>183</sup>  $\text{CuFeO}_2$  thin films have been prepared by techniques such as pulsed laser deposition (PLD) and radio-frequency (RF) sputtering.<sup>184-186</sup> However, these vacuum-based processes are complex and time consuming.  $\text{CuFeO}_2$  transparent thin-films prepared by a sol-gel route have produced promising conductivity ( $0.28 \text{ S cm}^{-1} - 0.36 \text{ S cm}^{-1}$ ) and hole mobility as well as a wide bandgap (3.38 eV).<sup>187</sup> Wang and co-workers were the first to report an application of C343 sensitized  $\text{CuFeO}_2$  thin-films as photocathodes in p-DSCs.<sup>190</sup> The sintering process and thickness of the  $\text{CuFeO}_2$  photocathode films were roughly optimized. A comparatively deeper valence band of  $\text{CuFeO}_2$  (0.69 V vs NHE) was found resulting in a larger  $V_{\text{OC}}$  (365 mV) compared to NiO. The overall PCE (0.01%) for the optimised device (2.8  $\mu\text{m}$ ) was however limited by poor  $J_{\text{SC}}$  ( $0.071 \text{ mA cm}^{-2}$ ), which was attributed to a low specific surface area ( $6.5 \text{ m}^2 \text{ g}^{-1}$ ).

To improve the photocurrent, the p-type conductivity of  $\text{CuFeO}_2$  powders have also been improved by  $\text{Mg}^{2+}$  or  $\text{Ni}^{2+}$  doping. The maximum p-type conductivity, until that point, of  $18 \text{ S cm}^{-1}$  was recorded for  $\text{CuFe}_{1-x}\text{Ni}_x\text{O}_2$  ( $x = 0.01, 0.02$  and  $0.03$ ) in the temperature range from 600 to 1000 K.<sup>188</sup>  $\text{CuFe}_{1-x}\text{Mg}_x\text{O}_2$  thin films have been synthesized by a sol-gel method.<sup>189</sup> In thin films of these materials, the resistivity first decreased to a minimum value (3.23  $\Omega$ ) observed at room temperature at  $x = 0.02$ , and then increased with increasing  $x$ .  $\text{CuFe}_{1-x}\text{Mg}_x\text{O}_2$  has also been prepared by hydrothermal synthesis, giving hexagonal platelets, which in p-DSCs were observed to enhance the lifetime of photoinduced charge carriers with respect to undoped

material.<sup>189</sup> The authors attribute the increase in lifetime to improved charge transport, due to the addition of Mg inducing more acceptor-type states, which increases the p-type carrier concentration and improves the conductivity of CuFeO<sub>2</sub>. In this study, the authors found that the optimum Mg content of 0.1% in CuFe<sub>1-x</sub>Mg<sub>x</sub>O<sub>2</sub> gave the longest lifetime for the photoinduced charge carriers, which was a 94% enhancement compared with the lifetime recorded for pure CuFeO<sub>2</sub>.

CuBO<sub>2</sub> was prepared by a sol-gel method and the as-obtained particles were applied in photocathodes for p-DSCs with DPP-NDI dye as the sensitizer and tris(4,40-ditert-butyl-2,20-bipyridine)cobalt(III/II) as the redox mediator. Consistent with a deeper valence band position compared with NiO, the CuBO<sub>2</sub> based p-DSC attained a V<sub>OC</sub> = 453 mV, which was 150 mV higher than the equivalent NiO-DSC under the same conditions. However, a low J<sub>SC</sub> (0.02 mA cm<sup>-2</sup>) arose due to a low specific surface area (18.5 m<sup>2</sup> g<sup>-1</sup>).<sup>191</sup>

In conclusion we can state that delafossite based materials are fairly promising substitutes for NiO as semiconductors in DSCs, in particular due to their valence band position in conjunction with a higher hole lifetime which leads to a higher V<sub>OC</sub>. However, they are yet to live up to their promise and there is still some optimization required, especially in terms of morphology and porosity. The most important issue of such semiconductors is their particle size, which can be improved trying different synthetic routes. This work has been already done for CuCrO<sub>2</sub>, obtaining particle size between 20-40 nm. However, the best result obtained with such semiconductor (ca. 0.3%) is far from the highest efficiency delivered with NiO. A way to improve the efficiency could be the employment of different dopant, such as iron, with CuCrO<sub>2</sub>. Also CuBO<sub>2</sub>, which presents a deeper valence band with respect to NiO, was not studied in detail and more work can be done in this direction.

#### 5.4 Oxyulfides

Hosono and co-workers have also proposed that high figure of merit p-type TCOs can be prepared by replacing oxygen with a chalcogen (S, Se, or Te), to introduce more delocalized *p*-orbitals.<sup>192</sup> Accordingly, LaCuOS and LaCuOSe p-type oxides have been synthesised.<sup>193,194</sup> Unfortunately, LaCuOSe has a too small band gap (ca. 2eV) for applications in p-DSCs. However, this strategy looks appealing as the *p* states of the chalcogen atoms are usually higher and therefore make the compound more prone to be *p*-doped. LaCuOS, has a higher hole mobility (~0.6 cm<sup>2</sup> V<sup>-1</sup> s<sup>-1</sup>), conductivity and optical transparency (60-70%) compared to NiO.<sup>193,194</sup> LaCuOS NPs synthesised by low temperature hydrothermal routes have a tendency to form La(OH)<sub>3</sub> and Cu<sub>x</sub>S mixtures. To hinder the formation of La(OH)<sub>3</sub>, a low temperature solvothermal method has been developed. The initial pH of solution was found to be crucial to tune the particle size (300 nm – 2 μm). However, LaCuOS thin-films sensitized with PMI-NDI showed a poor PCE (0.002%).<sup>195</sup> The authors attributed this to the similar valence band potentials of NiO and LaCuOS and reported that electron-hole recombination occurs rapidly which reduces the Fermi level under illumination, leading to low V<sub>OC</sub>. The authors also reported that the binding

affinity between dye and LaCuOS was weak and also hindered the device performance. The mixed chalcogen materials have shown promise, but there are clear synthetic challenges in controlling the composition and morphology of such materials. Consequently, there have been fewer reported devices incorporating these materials and ternary oxides are still a more appealing direction currently.

#### 5.5 Spinel structures

Another class of materials which could provide high conductivity are the spinels. Spinel structures (AB<sub>2</sub>O<sub>4</sub>) can exist in the forms; A<sup>II</sup>B<sub>2</sub><sup>III</sup>O<sub>4</sub> or A<sup>IV</sup>B<sub>2</sub><sup>II</sup>O<sub>4</sub> (2-3 and 4-2 spinels, respectively). Compared to binary NiO, spinel cobaltites (MCo<sub>2</sub>O<sub>4</sub>; M= Ni, Zn) possess richer redox chemistry and combine the actions from both metal (M) and Co ions. NiCo<sub>2</sub>O<sub>4</sub> is reported to have a higher conductivity, by at least two orders of magnitude compared to NiO.<sup>196</sup> NiCo<sub>2</sub>O<sub>4</sub> nanoparticles can be synthesised by co-precipitation, sol-gel, hydro/solvothermal, and simple chemical precipitation methods.<sup>196</sup> Li and co-workers have prepared NiCo<sub>2</sub>O<sub>4</sub> NPs by a hydrothermal route, modifying the process to obtain nanosheet, nanowires and nanowire-nanosheet arrays.<sup>196</sup> In particular, the nanowire-woven nanosheet arrays in conjunction with N719 dye produced a PCE = 0.785% (V<sub>OC</sub> = 189 mv, J<sub>SC</sub> = 8.35 mA cm<sup>-2</sup>, FF = 50%), which is a significant value among the p-DSCs fabricated using the standard I<sub>3</sub><sup>-</sup>/I<sup>-</sup> electrolyte. In the future, the focus could be to dope the NiCo<sub>2</sub>O<sub>4</sub> nanostructures to increase the conductivity and adjust the Fermi level energy. As far as we are aware, results on doping have not yet been reported and the material has not been tested with optimised photosensitizers for photocathodes. A very promising PCE close to 0.8% with spinels suggests that this should be a more fruitful direction of research. There is a significant chemical space to be explored in terms of structure, doping, stoichiometry etc. So far, there has been little follow up work in this area published and it will be interesting to see what develops in the near future.

#### 6. Device stability

Despite increasing effort towards improving p-type DSCs since 1999, there is a lack of consideration beyond efficiency at this stage in the development of these devices. Few papers mention the durability and chemical stability of their devices. The little knowledge that is at our disposal comes from n-type counterparts. Concerning electrolytes, for example, the iodide couple is known to degrade.<sup>197</sup> On the other hand, as reported by Gibson et al., the stability in the presence of a cobalt based redox mediator was pretty good.<sup>38</sup> In terms of semiconductors, it is established that CuO and Cu<sub>2</sub>O suffer from problems of instability over long term measurements. CuO is subjected to passivation<sup>198</sup> and Cu<sub>2</sub>O is well-known to be unstable in the presence of the electrolyte. On the other hand, as far as we know, delafossite and spinels are expected to be stable over time. So, despite some parallels that can be drawn from other photoelectrochemical systems, there is a need to investigate the stability of p-type DSCs in the presence of different dyes, with different anchoring groups, in order to evaluate and

improve issues such as desorption in the presence of the electrolyte. In general, if the kinetics are optimised, e.g. in a high-performing device, and species are not left in an excited or high-valence state for long, decomposition routes will be minimised.

### 7. Toward the increasing of p-type DSCs performance

Despite much progress in the field in the last 20 years, particularly in terms of mechanistic understanding, the reported PCEs of p-DSCs remain very low. Clearly, at the heart of the device, the optimisation of the dye will bring further improvements and most of the research in the field has been directed at engineering new structures and optimising the optical and electronic properties of the molecules. However, the rapid recombination at the dye-electrode interface still limits progress. The  $I_3^-/I^-$  electrolyte fundamentally limits the efficiency of the device, because of the large overpotential, particularly when tandem devices are constructed. The electrolytes are challenging to optimise, particularly one-electron, outer sphere shuttles, which are prone to low barriers to recombination at the working electrode surface. Furnishing the ligands with alkyl substituents to block recombination brings issues with diffusion in the pores, which requires optimisation of the electrode morphology. Slowing down the kinetics, such as moving from iron to cobalt or copper shuttles where there is a reorganizational energy barrier to electron transfer, is beneficial in terms of reducing recombination at the electrode/electrolyte interface, but this is typically accompanied by slower dye regeneration which leads to more recombination at the electrode/dye interface. Therefore, it is necessary to take a holistic approach and to investigate combinations of dyes and electrolytes together.

The real step-change in performance is likely to come from a new metal oxide, but this is arguably the hardest part to develop. Frequently there is a trade-off between conductivity and transparency and so finding a material with all the necessary credentials (a p-type equivalent of anatase) is not straightforward. The obvious candidates, which have been identified from theory, such as oxysulfides, delafossites and spinels have all been tested in p-type DSCs, but in each case, if the  $V_{oc}$  was improved, the current was sacrificed. There are a number of potential reasons, such as insufficient surface area for the dye to adsorb or insufficient porosity for the electrolyte to diffuse, which could be addressed through systematic studies. There could be issues associated with the physical properties such as the dielectric constant or surface properties, which could be addressed through applying novel architectures or layered materials. Alternatively, there could be a fundamental underlying issue which could be more challenging to address, such as inherent low mobility of holes or the band-structure itself. Certainly, without a systematic investigation of a wider pool of materials, progress will remain incremental. Fortunately, interest in photoelectrochemical approaches to solar energy conversion is increasing, particularly with the possibility to perform photocatalytic reactions at the electrode surfaces, such as the generation of solar fuels.

### 8. Tandem-DSCs

The ultimate purpose of a p-type DSC is to be used in tandem solar cells, to increase the spectral response of the cell without sacrificing the photovoltage. In a typical tandem DSC device, different dye molecules are adsorbed onto the surface of the two mesoporous thin-film of either the p-type semiconductor at the cathode or the n-type semiconductor at the anode. Photons exceeding the HOMO-LUMO gap can promote the dyes into an energetically excited state. Then, depending on the electrode, either; i) an electron is transferred (or "injected") from the sensitizer molecule into the conduction band (CB) of the n-type semiconductor or ii) an electron is transferred from the valence band (VB) of the p-type semiconductor to the photosensitizer, leaving a hole in the semiconductor. Charges migrate through the mesoporous photoelectrodes while the reduced and oxidised sensitizers are then regenerated by the redox mediator by electron transfer. Higher energy photons are collected at the top electrode, and lower energy photons, which would usually be transmitted are collected at the bottom electrode. Currently, n-type semiconductors give the best power conversion efficiency (PCE) for DSCs (14.7 %<sup>10</sup>) and, as a consequence, research in the field is dominated by n-type DSCs, particularly using  $TiO_2$  electrodes. The performance of p-n DSCs is limited by the comparatively poor performance of p-type DSCs at present.

The first tandem DSC was fabricated with a  $NiO|erythrosin\ B$  photocathode and a  $TiO_2|N3(cis-bis(isothiocyanato)bis(2,2'-bipyridyl-4,4'-dicarboxylato) ruthenium(II))$  photoanode.<sup>11</sup> The tandem cell successfully proved that the photovoltage of the p-n-DSC was close to the sum of the individual cells. On the other hand, the PCE and fill factor of the device was low (PCE = 0.39%, FF = 0.199), which was attributed to the limiting photocurrent at the photocathode ( $J_{sc} = 0.27\text{ mA cm}^{-2}$ ). Following this first example, Gibson et al., after optimization of p-type device, constructed a tandem DSCs, achieving a  $V_{oc}$  of 0.91 V, a FF of 0.62, and an efficiency of 0.55%.<sup>39</sup> The authors attributed this enhanced t-DSC performance to the suitability of the  $Co^{II/III}$  redox couple to both the  $NiO$ - and  $TiO_2$ -based semiconductors. More recently, Gibson et al. reported a tandem cells with up to  $5.2\text{ mA cm}^{-2}$ , employing CAD3 as p-type dye.<sup>48</sup> Tandem devices require current matching between the photoanode and photocathode, so the film thickness of the  $TiO_2$  electrode was reduced from the usual  $10\text{ }\mu\text{m}$  and current-voltage and IPCE measurements were taken until a current was obtained that matched the current that would be produced by the photocathode when positioned at the bottom of the cell. Bach et al. assembled a tandem device with a more encouraging efficiency ( $\eta = 2.42\%$ ).<sup>42</sup> This device incorporated the optimised donor-acceptor dye, PMI-nT-TPA, which provides control over the spatial separation of the photogenerated charge carriers. Very recently, Odobel and co-workers have produced a new series of diketopyrrolopyrrole (DPP)-based sensitizers which have performed well when combined with the conventional  $I_3^-/I^-$  electrolyte (Th-DPP-NDI  $J_{sc} = 7.38\text{ mA cm}^{-2}$ ;  $V_{oc} = 147\text{ mV}$ ; FF = 0.32;  $\eta = 0.35\%$ ).<sup>12</sup> This has enabled the fabrication of a highly efficient p-n junction DSC, in which the performance of

NiO|Th-DPP-NDI photocathode and TiO<sub>2</sub>|D35 photoanode was greater than that of the individual sub-devices ( $J_{sc} = 6.73 \text{ mA cm}^{-2}$ ;  $V_{oc} = 910 \text{ mV}$ ;  $\eta = 4.1 \%$ ).

In conclusion, despite low performances, improvements are now being made to the efficiency of tandem devices. The electrolyte has a crucial role, and has to match perfectly all the dyes involved in the process, both at the photocathode and the photoanode. In the long term, if efficiencies surpassing 20% are to be made, it will be necessary to find a new semiconductor which has a valence band at least 0.5 V lower than NiO, or replace TiO<sub>2</sub> with a material with a higher lying conduction band. Given that anatase already has the perfect balance of properties required for efficient DSCs, it is preferable that NiO is replaced with an appropriate p-type material. Given the challenges of finding transparent p-type semiconductors, this will require an intensive focus. However, the potential rewards are substantial.

## Conclusions

Over the last 20 years the performance of p-type DSCs has improved by a couple of orders of magnitude, due to the improvements made to the electrode materials, dyes and electrolytes. However, there are many unresolved questions in this area and there is a lack of a reliable benchmark system for comparing new components. The best electrolyte composition to use in p-type is not really defined as it is dependent on the dye structure employed. Cobalt based electrolytes have only been successful with dyes having a long-lived charge separated state and the iodine-based electrolyte presents several issues that have not yet been resolved. At the same time, there is not a well-defined set of conditions to test new materials. Each component of the device affects another, so it is not straightforward to predict the outcomes of simple substitutions. One reason for this is the complex kinetics and several mechanistic aspects are still not fully understood. Even the high-performing dyes tested in p-DSC, e.g. P1, CAD3 present short charge separated state lifetimes, which makes efficient dye-regeneration challenging to achieve. The reason behind this is not clear, despite several proposed explanations, including the possible interaction of iodine with semiconductor surface or forming a complex with the dye. The highest efficiency reached with PMI-6T-NDI dye and Fe(II/III) based electrolytes is equal to 2.51%, which is far from n-type DSC efficiency and could hamper the general efficiency of the device when employed in a t-DSC. The application of redox shuttles with faster dye regeneration kinetics, such as iron based complexes, and dyes with longer lifetimes for the charge separated state, of the order of microseconds, may further improve the performance. At the

same time, the discovery of a suitable semiconductor could be fundamental for the enhancement of device performance. Despite attempts to develop alternative materials to NiO, research is far from providing a satisfactory result. So, p-DSCs are limited owing to the lack of a suitable wide band gap p-type semiconductor with sufficient transparency and good charge transport properties. The discovery of p-type semiconductivity in degenerate n-type semiconductors could potentially solve this problem, provided that recombination losses can be curbed.

**Table 1.** Summarised photovoltaic performance of NiO based p-DSCs reported in the literature (with an I<sup>-</sup>/I<sub>3</sub><sup>-</sup> electrolyte).  $V_{oc}$  is the open-circuit voltage at the  $J = 0$  intercept,  $J_{sc}$  is the short-circuit current density at the  $V = 0$  intercept, FF is the device fill factor, PCE is the power conversion efficiency and IPCE is the monochromatic incident photon-to-current conversion efficiency.  $\tau(\text{NiO}^+/\text{dye}^-)$  is charge separated lifetime of dye on NiO calculated through time-resolved transient absorption measurements. <sup>a</sup> Not reported.

Dye	V <sub>oc</sub> (mV)	J <sub>sc</sub> (mA cm <sup>-2</sup> )	FF	PCE (%)	IPCE (%)	τ(NiO <sup>+</sup> /dye)	Ref.
Erythrosin B	95	1.016	0.40	0.039	8	- <sup>a</sup>	49
C343	0.117	0.88	0.28	0.036	- <sup>a</sup>	20 ps	36
P1	84	5.48	0.34	0.15	64	2.7 ps, 17 ps, 205 ps	41
P2	63	3.37	0.31	0.07	32	- <sup>a</sup>	79
Bodipy-Co <sub>2</sub> H	95	1.48	0.36	0.05	20	4.1 ps	77
Bodipy 4	97	1.6	0.38	0.06	27	5 ps	77
Bodipy 5	109	3.7	0.35	0.14	44	0.1 ps, 13 ps	77
Bodipy 6	95	1.58	0.35	0.05	23	12 ps, 12 ns	76,77
Bodipy 7	106	5.78	0.31	0.2	24	4.9 ps, 580 ps	77
P3	55	1.36	0.34	0.03	6	2.4 ps, 20 ps, 317 ps	79
P7	80	3.37	0.35	0.09	26	- <sup>a</sup>	79
CAD3	101	8.21	0.31	0.25	50	1.2 ns	48
P4	100	2.48	0.36	0.09	44	- <sup>a</sup>	40
CAD1	87	3.32	0.33	0.09	25	300 ps	52
CAD2	96	3.25	0.33	0.1	17	100 ps	52
T3	121	5.01	0.3	0.184	27	- <sup>a</sup>	53
T3H	133	5.57	0.31	0.23	25	- <sup>a</sup>	55
T5	124	4.51	0.33	0.186	23	- <sup>a</sup>	53
T6	133	4.02	0.33	0.178	22	- <sup>a</sup>	53
T4	152	3.94	0.35	0.21	22	- <sup>a</sup>	55
T4H	152	6.74	0.31	0.32	26	- <sup>a</sup>	55
BH2	97	4.30	0.31	0.13	- a	- <sup>a</sup>	56
BH4	128	7.40	0.3	0.28	- a	- <sup>a</sup>	56
BH6	95	4.40	0.31	0.13	- a	- <sup>a</sup>	56
Th-DPP	74	0.26	0.53	0.008	< 2	- <sup>a</sup>	12
Th-DPP-NDI	147	7.38	0.32	0.35	55	- <sup>a</sup>	12
DPP-Br	125	0.75	0.37	0.03	8	8.6 ps, 75 ps	64
DPPCN <sub>2</sub>	135	1.51	0.32	0.07	22	- <sup>a</sup>	12
DPP-NDI	155	1.38	0.40	0.09	25	13 ps, 260 ps , 140μs	64
TPA-DPP	81	0.70	0.25	0.01	5	- <sup>a</sup>	12
TPA-DPP-NDI	123	4.04	0.32	0.16	30	- <sup>a</sup>	12
ISO-Br	87	0.82	0.34	0.025	7	- <sup>a</sup>	66
ISO-NDI	96	1.27	0.33	0.04	5	- <sup>a</sup>	66
PMI-2T-TPA	153	2.06	0.29	0.09	- a	177 ns, 1.34 μs	42
PMI-4T-TPA	176	3.40	0.32	0.19	- a	1.22μs, 12.2μs	42
PMI-6T-TPA	218	5.35	0.35	0.41	- a	2.54 μs, 13.6 μs	42
PMI-NDI	120	1.76	0.35	0.073	32	5 μs, 50 μs	38
PMI-PhNDI	130	1.64	0.35	0.074	43	3 μs, 55 μs	38
PMI-PhC <sub>60</sub>	95	1.88	0.32	0.058	31	2.4 μs	38

zzx-pp1	96	5.70	0.38	0.207	50	..a	50
zzx-op1-2	117	7.57	0.41	0.353	70	..a	50
zzx-op1-3	115	6.68	0.4	0.308	58	..a	50
zzx-op2	111	4.00	0.36	0.16	48	..a	51
zzx-op3	109	3.80	0.36	0.15	42	..a	51
Fielden-1	50	0.83	0.43	0.018	14	..a	71
Fielden-2	49	0.87	0.32	0.014	11	..a	71
Fielden-3	66	0.83	0.33	0.018	14	..a	71
Fielden-4	1.11	0.86	0.37	0.036	13	..a	71
Fielden-5	70	0.84	0.37	0.014	10	..a	71
CW1	99	2.66	0.35	0.093	25	..a	72
CW2	118	4.05	0.34	0.16	40	..a	72
BAI-COOH	79	1.13	0.33	0.029	8	..a	67
RBG-174	90	2.88	0.37	0.096	..a	..a	63
COCO	91	2.45	0.36	0.080	..a	..a	63
BBTX	88	4.32	0.33	0.126	..a	..a	63
COCN	77	1.53	0.32	0.038	..a	..a	63
CB <sub>5</sub>	115	1.52	0.34	0.059	9	..a	78
CB <sub>6</sub>	117	1.13	0.31	0.044	4	..a	78
CB <sub>7</sub>	117	2	0.33	0.076	11	..a	78
CB <sub>8</sub>	118	1.71	0.33	0.066	7	..a	78
W1	131	2.83	0.34	0.126	13	..a	57
W2	121	4.16	0.33	0.166	17	..a	57
W3	134	2.32	0.33	0.103	8	..a	57
O6	97	1.04	0.37	0.037	14	..a	58
O7	90	1.74	0.38	0.06	18	..a	58
O2	94	1.43	0.37	0.05	12	..a	58
QT-1	120	8.20	0.34	0.33	57	..a	60
Lin-1	113	1.38	0.34	0.05	14	..a	61
Lin-5	122	2.18	0.35	0.09	17	..a	61
p-SQ1	117	1.22	0.37	0.056	6	-a	59
p-SQ2	140	1.92	0.42	0.113	18	-a	59
SQ	85	1.18	0.34	0.034	3	2.2 ps, 53ps	62
SQ-PMI	65	1.31	0.35	0.026	5	3 ps, 112 ps	62
SQ-PMI-NDI	95	2.73	0.32	0.083	25	4.8ps,130ps	62
SL1	104	2.25	0.34	0.079	18	..a	31
SL2	77	1.50	0.33	0.038	7	..a	31
K1	96	2.91	0.32	0.09	14	..a	26
K2	93	1.96	0.39	0.07	9	..a	26
O3	100	2.75	0.36	0.10	..a	1.1 ns	28
O13	89	2.66	0.31	0.074	..a	..a	27
O18	93	3.43	0.33	0.104	..a	1.7 ns	28
O17	92	2.69	0.34	0.085	..a	..a	27
O8	63	0.44	0.36	0.009	2	0.15ps, 8.91 ps	30

						0.25 ns	
<b>O11</b>	82	1.84	0.34	0.051	9	0.43ps, 24.1ps 0.63 ns	<sup>30</sup>
<b>O12</b>	79	1.16	0.36	0.033	5	2.63 ns, 52.9ns 1.13 ns	<sup>30</sup>
<b>ZnP</b>	98	0.19	0.35	0.006	- <sup>a</sup>	51.7 ps	<sup>68</sup>
<b>ZnP-NDI</b>	127	1.38	0.32	0.056	- <sup>a</sup>	219 ps	<sup>68</sup>
<b>Zn-TCPP</b>	120	0.5	0.4	0.02	10	- <sup>a</sup>	<sup>69</sup>
<b>ZnP-TCPP-C<sub>60</sub>PPy</b>	146	1.4	0.4	0.08	35	- <sup>a</sup>	<sup>69</sup>
<b>Zn-1</b>	57	0.28	0.35	0.006	5	15 ps, 190 ps, 1 ns	<sup>75</sup>
<b>Zn-2</b>	74	0.45	0.35	0.012	8	32 ps, 1.6 ns	<sup>75</sup>
<b>Zn-3</b>	76	0.51	0.37	0.014	10	210 ps, 2.3 ns	<sup>75</sup>
<b>Zn-3-C<sub>60</sub>PPy</b>	80	0.55	0.35	0.015	- <sup>a</sup>	350 ps, 5 ns	<sup>75</sup>
<b>[Ru(bpy)<sub>2</sub>(H1)]</b>	95	4.06	0.36	0.139	- <sup>a</sup>	- <sup>a</sup>	<sup>29</sup>
<b>[Ru(dcb)<sub>3</sub>]<sup>2+</sup></b>	110	0.09	0.43	0.004	- <sup>a</sup>	5.1 μs	<sup>87</sup>
<b>[Ru(dcb)<sub>2</sub>(NMI-phen)]<sup>2+</sup></b>	95	0.16	0.36	0.006	- <sup>a</sup>	14 μs	<sup>87</sup>
<b>IrPhen</b>	345	0.14	0.44	0.021	- <sup>a</sup>	50-70 ns, 1μs, 5-30 μs	<sup>33</sup>
<b>IrDPQCN2</b>	508	0.25	0.54	0.068	- <sup>a</sup>	50-70 ns, 1μs, 5-30 μs	<sup>33</sup>
<b>IrBpystyryl</b>	383	0.37	0.44	0.061	- <sup>a</sup>	50-70 ns, 1μs, 5-30 μs	<sup>33</sup>
<b>AS9</b>	90	0.68	0.36	0.022	4	- <sup>a</sup>	<sup>34</sup>
<b>AS10</b>	90	0.66	0.37	0.022	3	- <sup>a</sup>	<sup>34</sup>
<b>AS11</b>	70	0.45	0.38	0.013	2	- <sup>a</sup>	<sup>34</sup>
<b>AS12</b>	90	0.36	0.4	0.013	2	- <sup>a</sup>	<sup>34</sup>
<b>AS13</b>	100	0.82	0.39	0.032	8	- <sup>a</sup>	<sup>34</sup>
<b>AS14</b>	100	1.12	0.37	0.043	10	- <sup>a</sup>	<sup>34</sup>

**Table 2.** Selection of reported parameters for various p-type metal-oxide semiconductors which have also been utilized in p-type dye-sensitized solar cells. Exact values can differ depending on synthesis methods and testing conditions used.

p-type semiconductor	Structure	Space Group	Transparency (%)	Band gap (eV)	Valance Band Energy (eV vs. Vacuum)	Flatband potential (V vs. SCE)	Dielectric constant	Conductivity (S cm <sup>-1</sup> )	Carrier Concentration (cm <sup>-3</sup> )	Hole mobility (cm <sup>2</sup> V <sup>-1</sup> s <sup>-1</sup> )
NiO	cubic	Fm3m	40 <sup>199</sup>	3.4 - 4.3 <sup>200</sup>	-5.04 <sup>122</sup>	0.1 V at pH 9.4 <sup>191</sup>	9.7 <sup>21</sup>	10 <sup>-4</sup> <sup>202</sup>	5.00 × 10 <sup>16</sup> - 1 × 10 <sup>20</sup> <sup>203</sup>	0.141 <sup>204</sup>
CuO	monoclinic	C2/c <sup>205</sup>	55 <sup>206</sup>	1.3 - 2.1 <sup>207</sup>	-5.57 <sup>191</sup>	0.15 - 0.41 V at pH 9.4 <sup>191</sup>	18.1 <sup>201</sup>	3.85 <sup>206</sup>	1.5 × 10 <sup>16</sup> - 7.4 × 10 <sup>19</sup> <sup>199</sup>	0.12 <sup>206</sup>
Cu <sub>2</sub> O	cubic	Pn3m	72 <sup>206</sup>	2.1 - 2.6 <sup>206</sup>	-5.69 <sup>206</sup>	-0.22 V <sup>208</sup>	12 <sup>209</sup>	6.7×10 <sup>-3</sup> <sup>206</sup>	1.5 × 10 <sup>15</sup> - 5.7 × 10 <sup>19</sup> <sup>206,208</sup>	51 <sup>206</sup>
CuGaO <sub>2</sub>	delafossite, rhombohedral	R-3m <sup>210</sup>	80 <sup>211</sup>	3.6 - 3.9 <sup>211,212</sup>	-5.29 <sup>172</sup>	0.49 V at pH 6.3 <sup>202</sup>	0.96 <sup>213</sup>	10 <sup>-1</sup> - 10 <sup>-2</sup> <sup>202</sup>	1.7 × 10 <sup>18</sup> - 3.5 × 10 <sup>20</sup> <sup>213</sup>	0.23 <sup>211</sup>
CuCrO <sub>2</sub>	delafossite	R-3m	77 <sup>214</sup>	3.0 <sup>211</sup>	-5.3 <sup>121</sup>	0.21 V <sup>215</sup>	0.2 - 0.6 <sup>216</sup>	0.23 <sup>217</sup>	5.06 × 10 <sup>14</sup> <sup>215</sup>	0.2 <sup>191</sup>
NiCo <sub>2</sub> O <sub>4</sub>	Spinel	Fd3m	80 <sup>218</sup>	2.06 - 3.63 <sup>219</sup>	-5.3 <sup>218</sup>	0.14 V <sup>220</sup>	N/A	4 <sup>218</sup>	N/A	N/A
CuAlO <sub>2</sub>	delafossite, rhombohedral	R-3m	75 <sup>221</sup>	3.55 <sup>211</sup>	-5.2 <sup>222</sup>	0.445 V at pH 7.2 <sup>223</sup>	10 <sup>224</sup>	3×10 <sup>-1</sup> <sup>221</sup>	1.3 × 10 <sup>17</sup> <sup>225</sup>	10 <sup>191</sup>
CuFeO <sub>2</sub>	delafossite, hexagonal	R-3m	50 <sup>226</sup>	1.5 - 3.38 <sup>227,228</sup>	-5.3 <sup>227</sup>	0.82 V <sup>227</sup>	20 <sup>227</sup>	0.36 <sup>228</sup>	5.3 × 10 <sup>18</sup> <sup>228</sup>	0.2 <sup>227</sup>
CuBO <sub>2</sub>	delafossite, hexagonal	R-3m	70 <sup>191</sup>	4.0 <sup>229</sup>	-5.9 <sup>230</sup>	0.31 V at pH 9.4 <sup>191</sup>	N/A	1.65 <sup>229</sup>	3.07 × 10 <sup>13</sup> <sup>191</sup>	100 <sup>19</sup>
LaCuOS	tetragonal	P4/nmm <sup>231</sup>	70 <sup>232</sup>	3.1 <sup>233</sup>	-5.0 <sup>234</sup>	0.26 - 0.4 V at pH 6.3 <sup>234</sup>	4 <sup>231</sup>	1.2×10 <sup>-2</sup> <sup>232</sup>	1 × 10 <sup>19</sup> <sup>194</sup>	0.6 <sup>234</sup>
K:ZnO	wurtzite, hexagonal	P63mc	85 <sup>159</sup>	3.23 <sup>159</sup>	-5.7 <sup>159</sup>	1.04 V <sup>159</sup>	N/A	N/A	1.9 × 10 <sup>16</sup> <sup>157</sup>	2.6 × 10 <sup>-3</sup> <sup>159</sup>
In <sub>2</sub> O <sub>5</sub> Sn (ITO)	Cubic	Ia3	80 <sup>236</sup>	4.1 <sup>235</sup>	-4.7 <sup>237</sup>	-1.5 V <sup>238</sup>	3.34 <sup>239</sup>	104 <sup>236</sup>	5 × 10 <sup>20</sup> <sup>240</sup>	39 <sup>241</sup>

## Conflicts of interest

There are no conflicts to declare.

## Acknowledgements

We thank Newcastle University for a PhD studentship for GHS; the EPSRC for studentship for FAB (EPJ5002881); The North East Centre for Energy Materials EP/R021503/1; JM, EB and EAG thank the ERC, starting grant, p-TYPE 715354.

## Notes and references

- 1 U.S. Energy Information Administration, International Energy Outlook 2018.
- 2 N.S Lewis, D.G. Nocera *Proc Natl Acad Sci U S A*, 2006, **103**, 15729–15735.
- 3 P. M. Cox, R. A. Betts, C. D. Jones, S. A. Spall and I. J. Totterdell, *Nature*, 2000, **408**, 184–187.
- 4 T. L. Root, J. T. Price, K. R. Hall, S. H. Schneider, C. Rosenzweig and J. A. Pounds, *Nature*, 2003, **421**, 57–60.
- 5 European Commission, The roadmap for transforming the EU into a competitive, low-carbon economy by 2050, 2011.
- 6 N. S. Lewis, G. Crabtree, A. J. Nozik, M. R. Wasielewski, P. Alivisatos, H. Kung, J. Tsao, E. Chandler, W. Walukiewicz, M. Spitler, R. Ellingson, R. Overend, J. Mazer, M. Gress, J. Horwitz, C. Ashton, B. Herndon, L. Shapard and R. M. Nault, Basic Research Needs for Solar Energy Utilization. Report of the Basic Energy Sciences Workshop on Solar Energy Utilization, April 18–21, 2005, Office of Science, U.S. Department of Energy 2005.
- 7 K. Yoshikawa, H. Kawasaki, W. Yoshida, T. Irie, K. Konishi, K. Nakano, T. Uto, D. Adachi, M. Kanematsu, H. Uzu and K. Yamamoto, *Nat. Energy*, 2017, **2**, 17032.
- 8 S. Ruhle, *Sol Energy*, 2016, **130**, 139–147.
- 9 M. Freitag, J. Teuscher, Y. Saygili, X. Zhang, F. Giordano, P. Liska, J. Hua, S. M. Zakeeruddin, J.-E. Moser, M. Grätzel and A. Hagfeldt, *Nat. Photonics*, 2017, **11**, 372–378.
- 10 K. Kakiage, Y. Aoyama, T. Yano, K. Oya, J. Fujisawa and M. Hanaya, *Chem. Commun.*, 2015, **51**, 15894–15897.
- 11 J. J. He, H. Lindstrom, A. Hagfeldt and S. E. Lindquist, *Sol. Energ. Mater. Sol. C*, 2000, **62**, 265–273.
- 12 Y. Farre, M. Raissi, A. Fihey, Y. Pellegrin, E. Blart, D. Jacquemin and F. Odobel, *ChemSusChem*, 2017, **10**, 2618–2625.
- 13 J. J. He, H. Lindstrom, A. Hagfeldt and S. E. Lindquist, *J. Phys. Chem. B*, 1999, **103**, 8940–8943.
- 14 E. A. Gibson, L. Le Pleux, J. Fortage, Y. Pellegrin, E. Blart, F. Odobel, A. Hagfeldt and G. Boschloo, *Langmuir*, 2012, **28**, 6485–6493.
- 15 Y. Pellegrin, L. Le Pleux, E. Blart, A. Renaud, B. Chavillon, N. Szuwarski, M. Boujtita, L. Cario, S. Jobic, D. Jacquemin and F. Odobel, *J. Photoch. Photobiol. A*, 2011, **219**, 235–242.
- 16 F. Brunner, N. Marinakis, C. Wobill, M. Willgert, C. D. Ertl, T. Kosmalski, M. Neuburger, B. Bozic-Weber, T. Glatzel, E. C. Constable and C. E. Housecroft, *J. Mater. Chem. C*, 2016, **4**, 9823–9833.
- 17 J. Cui, J. F. Lu, X. B. Xu, K. Cao, Z. Wang, G. Alemu, H. L. Yuang, Y. Shen, J. Xu, Y. B. Cheng and M. K. Wang, *J. Phys. Chem. C*, 2014, **118**, 16433–16440.
- 18 Y. W. Dong, L. G. Wei, R. Q. Fan, Y. L. Yang and P. Wang, *RSC Adv.*, 2016, **6**, 39972–39981.
- 19 G. Alemu, J. Cui, K. Cao, J. P. Li, Y. Shen and M. K. Wang, *RSC Adv.*, 2014, **4**, 51374–51380.
- 20 F. Odobel, Y. Pellegrin, E. A. Gibson, A. Hagfeldt, A. L. Smeigh and L. Hammarstrom, *Coordin. Chem. Rev.*, 2012, **256**, 2414–2423.
- 21 F. Odobel and Y. Pellegrin, *J. Phys. Chem. Lett.*, 2013, **4**, 2551–2564.
- 22 M. Buchalska, J. Kunczewicz, E. Swietek, P. Labuz, T. Baran, G. Stochel and W. Macyk, *Coordin. Chem. Rev.*, 2013, **257**, 767–775.
- 23 A. Nattestad, M. Ferguson, R. Kerr, Y. B. Cheng and U. Bach, *Nanotechnology*, 2008, **19**, 295304.
- 24 J. N. Clifford, E. Palomares, M. K. Nazeeruddin, M. Gratzel and J. R. Durrant, *J. Phys. Chem. C*, 2007, **111**, 6561–6567.
- 25 P. Qin, H. J. Zhu, T. Edvinsson, G. Boschloo, A. Hagfeldt and L. C. Sun, *J. Am. Chem. Soc.*, 2008, **130**, 8570–8571.
- 26 C. J. Wood, K. C. D. Robson, P. I. P. Elliott, C. P. Berlinguette and E. A. Gibson, *RSC Adv.*, 2014, **4**, 5782–5791.
- 27 Z. Q. Ji, G. Natu and Y. Y. Wu, *ACS Appl. Mater. Inter.*, 2013, **5**, 8641–8648.
- 28 M. F. He, Z. Q. Ji, Z. J. Huang and Y. Y. Wu, *J. Phys. Chem. C*, 2014, **118**, 16518–16525.
- 29 N. Marinakis, M. Willgert, E. C. Constable and C. E. Housecroft, *Sustain. Energ. Fuels*, 2017, **1**, 626–635.
- 30 Z. Q. Ji, G. Natu, Z. J. Huang, O. Kokhan, X. Y. Zhang and Y. Y. Wu, *J. Phys. Chem. C*, 2012, **116**, 16854–16863.
- 31 S. Lyu, Y. Farre, L. Ducasse, Y. Pellegrin, T. Toupance, C. Olivier and F. Odobel, *RSC Adv.*, 2016, **6**, 19928–19936.
- 32 L. Zhang, J.M. Cole, *ACS Appl. Mater. Interfaces*, 2015, **7**, 3427–3455.
- 33 M. Gennari, F. Legalite, L. Zhang, Y. Pellegrin, E. Blart, J. Fortage, A. M. Brown, A. Deronzier, M. N. Collomb, M. Boujtita, D. Jacquemin, L. Hammarstrom and F. Odobel, *J. Phys. Chem. Lett.*, 2014, **5**, 2254–2258.
- 34 A. Sinopoli, C. J. Wood, E. A. Gibson and P. I. P. Elliott, *Dyes and Pigments*, 2017, **140**, 269–277.
- 35 E.A Gibson et al. *Polyhedron*, 2018, **140**, 109–115
- 36 A. Morandeira, G. Boschloo, A. Hagfeldt and L. Hammarstrom, *J. Phys. Chem. B*, 2005, **109**, 19403–19410.
- 37 A. Morandeira, J. Fortage, T. Edvinsson, L. Le Pleux, E. Blart, G. Boschloo, A. Hagfeldt, L. Hammarstrom and F. Odobel, *J. Phys. Chem. C*, 2008, **112**, 1721–1728.
- 38 L. Le Pleux, A. L. Smeigh, E. Gibson, Y. Pellegrin, E. Blart, G. Boschloo, A. Hagfeldt, L. Hammarstrom and F. Odobel, *Energ. Environ. Sci.*, 2011, **4**, 2075–2084.
- 39 E. A. Gibson, A. L. Smeigh, L. Le Pleux, J. Fortage, G. Boschloo, E. Blart, Y. Pellegrin, F. Odobel, A. Hagfeldt and L. Hammarstrom, *Angew. Chem. Int. Ed.*, 2009, **48**, 4402–4405.
- 40 P. Qin, M. Linder, T. Brinck, G. Boschloo, A. Hagfeldt and L. C. Sun, *Adv. Mater.*, 2009, **21**, 2993–2996.
- 41 L. Li, E. A. Gibson, P. Qin, G. Boschloo, M. Gorlov, A. Hagfeldt and L. C. Sun, *Adv. Mater.*, 2010, **22**, 1759–1762.
- 42 A. Nattestad, A. J. Mozer, M. K. R. Fischer, Y. B. Cheng, A. Mishra, P. Bauerle and U. Bach, *Nat. Mater.*, 2010, **9**, 31–35.
- 43 M. Awais, E. Gibson, E.J.G. Vos, D.P. Dowling, A. Hagfeldt, D. Dini, *Chemelectrochem*, 2014, **1**, 384–391.
- 44 S. Powar, T. Daeneke, M. T. Ma, D. C. Fu, N. W. Duffy, G. Gotz, M. Weidelener, A. Mishra, P. Bauerle, L. Spiccia and U. Bach, *Angew. Chem. Int. Ed.*, 2013, **52**, 602–605.
- 45 I. R. Perera, T. Daeneke, S. Makuta, Z. Yu, Y. Tachibana, A. Mishra, P. Bauerle, C. A. Ohlin, U. Bach and L. Spiccia, *Angew. Chem. Int. Ed.*, 2015, **54**, 3758–3762.
- 46 M. Liang and J. Chen, *Chem. Soc. Rev.*, 2013, **42**, 3453–3488.
- 47 J. Wang, K. Liu, R. R. Xing and X. H. Yan, *Chem. Soc. Rev.*, 2016, **45**, 5589–5604.
- 48 C. J. Wood, G. H. Summers and E. A. Gibson, *Chem. Commun.*, 2015, **51**, 3915–3918.

- 49 Q. Q. Zhang, K. J. Jiang, J. H. Huang, C. W. Zhao, L. P. Zhang, X. P. Cui, M. J. Su, L. M. Yang, Y. L. Song and X. Q. Zhou, *J. Mater. Chem. A*, 2015, **3**, 7695-7698.
- 50 Z. H. Liu, W. H. Li, S. Topa, X. B. Xu, X. W. Zeng, Z. X. Zhao, M. K. Wang, W. Chen, F. Wang, Y. B. Cheng and H. S. He, *ACS Appl. Mater. Inter.*, 2014, **6**, 10614-10622.
- 51 Z. H. Liu, D. H. Xiong, X. B. Xu, Q. Arooj, H. Wang, L. Y. Yin, W. H. Li, H. Z. Wu, Z. X. Zhao, W. Chen, M. K. Wang, F. Wang, Y. B. Cheng and H. S. He, *ACS Appl. Mater. Inter.*, 2014, **6**, 3448-3454.
- 52 C. J. Wood, M. Cheng, C. A. Clark, R. Horvath, I. P. Clark, M. L. Hamilton, M. Towrie, M. W. George, L. C. Sun, X. C. Yang and E. A. Gibson, *J. Phys. Chem. C*, 2014, **118**, 16536-16546.
- 53 F. Wu, S. B. Zhao, C. Zhong, Q. L. Song and L. N. Zhu, *RSC Adv.*, 2015, **5**, 93652-93658.
- 54 L. N. Zhu, H. B. Yang, C. Zhong and C. M. Li, *Dyes and Pigments*, 2014, **105**, 97-104.
- 55 F. Wu, L. N. Zhu, S. B. Zhao, Q. L. Song and C. L. Yang, *Dyes and Pigments*, 2016, **124**, 93-100.
- 56 K. A. Click, D. R. Beauchamp, B. R. Garrett, Z. J. Huang, C. M. Hadad and Y. Y. Wu, *Phys. Chem. Chem. Phys.*, 2014, **16**, 26103-26111.
- 57 F. Wu, J. L. Liu, X. Li, Q. L. Song, M. Wang, C. Zhong and L. N. Zhu, *Eur. J. Org. Chem.*, 2015, **31**, 6850-6857.
- 58 Z. Q. Ji, G. Natu, Z. J. Huang and Y. Y. Wu, *Energ. Environ. Sci.*, 2011, **4**, 2818-2821.
- 59 C. H. Chang, Y. C. Chen, C. Y. Hsu, H. H. Chou and J. T. Lin, *Org. Lett.*, 2012, **14**, 4726-4729.
- 60 Q.-Q. Zhang, K.-J. Jiang, J.-H. Huang, C.-W. Zhao, L.-P. Zhang, X.-P. Cui, M.-J. Su, L.-M. Yang, Y.-L. Song and X.-Q. Zhou, *J. Mater. Chem. A*, 2015, **3**, 7695-7698.
- 61 Y. S. Yen, W. T. Chen, C. Y. Hsu, H. H. Chou, J. T. Lin and M. C. P. Yeh, *Org. Lett.*, 2011, **13**, 4930-4933.
- 62 J. Warnan, J. Gardner, L. Le Pleux, J. Petersson, Y. Pellegrin, E. Blart, L. Hammarstrom and F. Odobel, *J. Phys. Chem. C*, 2014, **118**, 103-113.
- 63 R. Brisse et al. *Sustainable Energy Fuels*, 2018, **2**, 648-654.
- 64 Y. Farré, L. Zhang, Y. Pellegrin, A. Planchat, E. Blart, M. Boujtita, L. Hammarström, D. Jacquemin and F. Odobel, *J. Phys. Chem. C*, 2016, **120**, 7923-7940.
- 65 J. Cui, J. Lu, X. Xu, K. Cao, Z. Wang, G. Alemu, H. Yuang, Y. Shen, J. Xu, Y. Cheng and M. Wang, *J. Phys. Chem. C*, 2014, **118**, 16433-16440.
- 66 D. Ameline, S. Diring, Y. Farre, Y. Pellegrin, G. Naponiello, E. Blart, B. Charrier, D. Dini, D. Jacquemin and F. Odobel, *RSC Adv.*, 2015, **5**, 85530-85539.
- 67 G. H. Summers and E. A. Gibson, *ChemPhotoChem*, 2018, **2**, 498-506
- 68 L. Zhang et al. *RSC Adv.*, 2016, **6**, 77184-77194.
- 69 H. Tian et al. *Sci. Rep.*, 2014, **4**, 4282.
- 70 A. Maufroy, L. Favereau, FB Anne FB, Y. Pellegrin, E. Blart, M. Hissler, D. Jacquemin, F. Odobel, *J. Mater. Chem. A*, 2015, **3**, 3908-3917.
- 71 A.R. Marri, F.A. Black, J. Mallows, E.A. Gibson, J. Fielden, *Dyes and Pigments*, 2019, **165**, 508-517.
- 72 J. Cui, J. Lu, X. Xu, K. Cao, Z. Wang, G. Alemu, H. Yuang, Y. Shen, J. Xu, Y. Cheng, M. Wang, *J. Phys. Chem. C*, 2014, **118**, 16433-40.
- 73 H. Yamada, H. Imahori, Y. Nishimura, I. Yamazaki, S. Fukuzumi, *Adv. Mater.*, 2002, **14**, 892-895.
- 74 H. Yamada, H. Imahori, Y. Nishimura, I. Yamazaki, T.K. Ahn, S.K. Kim, D. Kim, S. Fukuzumi, *J. Am. Chem. Soc.*, 2002, **125**, 9129-9139.
- 75 E. Benazzi, G.H. Summers, F.A. Black, I.V. Sazanovich, I.P. Clark, E.A. Gibson, *Philosophical Transactions of the Royal Society A: Mathematical, Physical and Engineering Sciences*, 2019, DOI: 10.1098/rsta.2018.0338.
- 76 J. F. Lefebvre, X. Z. Sun, J. A. Calladine, M. W. George and E. A. Gibson, *Chem. Commun.*, 2014, **50**, 5258-5260.
- 77 E.A Gibson et al. *Phys. Chem. Chem.Phys*, 2016, **18**, 1059-1070.
- 78 M. Bonomo, A. Di Carlo, R. Centore, D. Dini and A. Carella, *Sol. Energy*, 2018, **169**, 237-241.
- 79 P. Qin, J. Wiberg, E.A.Gibson, M. Linder, L. Li, T. Brinck, A. Hagfeldt, B. Albinsson, L. Sun, *J. Phys. Chem. C*, 2010, **114**, 4738-4748.
- 80 A. L. Smeigh, A. L. Le Pleux, J. Fortage, Y. Pellegrin, E. Blart, F. Odobel, L. Hammarstrom, *Chem. Commun.*, 2012, **48**, 678-80.
- 81 L. Zhang, L. Favereau, Y. Farre, E. Mijangos, Y. Pellegrin, E. Blart, F. Odobel, L. Hammarstrom, *Phys. Chem. Chem. Phys.*, 2016, **18**, 18515-27.
- 82 L. D'Amario, L. J. Antila, B. Pettersson Rimgard, G. Boschloo, L. Hammarström, *Phys. Chem. Lett.*, 2015, **6**, 779-783.
- 83 R.J. Dillon, L. Alibabaei, T.J. Meyer, J.M. Papanikolas, *ACS Appl. Mater. Interfaces*, 2017, **9**, 26786-26796.
- 84 P. Lunkenheimer, A. Loidl, C.R. Ottermann, K.Bange, *Phys. Rev. B*, 1991, **44**, 5927-5930.
- 85 L. D'Amario, R. Jiang, U.B. Cappel, E.A. Gibson, G. Boschloo, H. Rensmo, L. Sun, L. Hammarstrom, H. Tian, *ACS Appl. Mater. Interfaces*, 2017, **9**, 33470-33477.
- 86 A. Morandeira, G. Boschloo, A. Hagfeldt, L. Hammarstrom, *J. Phys. Chem. B*, 2005, **109**, 19403-19410.
- 87 J.C. Freys, J.M.Gardner, L. D'Amario, A.M. Brown, L. Hammarstrom, *Dalton Trans.* 2012, **41**, 13105-13111.
- 88 A. Hagfeldt et al., *Chem. Rev.*, 2010, **110**, 6595-6663.
- 89 C.J. Wood, C.A.McGregor, E.A.Gibson, *ChemElectroChem*, 2016, **3**, 1827-1836.
- 90 C.S. Ponceca, P.Chabera, J.Uhlig, P.Persson, V. Sundstrom, *Chem. Rev.*, 2017, **117**, 10940-11024.
- 91 M. Abdellah, A.M. El-Zohry, L.J. Antila, C.D. Windle, E. Reisner, L. Hammarstrom, *J. Am. Chem. Soc.*, 2017, **139**, 1226-1232.
- 92 F. A. Black, C.J. Wood, S. Ngwerume, G.H. Summers, I.P. Clark, M.Towrie, J.E. Camp, E.A. Gibson, *Faraday Discuss.*, 2017, **198**, 449-461.
- 93 F.A. Black, C.A. Clark, G.H. Summers, I.P. Clark, M. Towrie, T. Penfold, M.W. George, E.A. Gibson, *Phys. Chem. Chem. Phys.*, 2017, **19**, 7877-7885.
- 94 G. Boschloo et al. *J. Phys Chem. C*, 2007, **111**, 17455-17458
- 95 M. Quintana, T. Edvinsson, A. Hagfeldt, G. Boschloo, *J. Phys. Chem. C*, 2007, **111**, 1035-1041.
- 96 S. Mori, S. Fukuda, S. Sumikura, Y. Takeda, Y. Tamaki, E. Suzuki, T. Abe, *J. Phys. Chem. C*, 2008, **112**, 16134-16139.
- 97 L. Li, E.A. Gibson, P. Qin, G.Boschloo, M.Gorlov, A. Hagfeldt, L.& Sun, *Adv. Mater.*, 2010, **22**, 1759-1762.
- 98 G. Natu, P. Hasin, Z. J. Huang, Z. Q. Ji, M. F. He and Y. Y. Wu, *ACS Appl. Mater. Inter.*, 2012, **4**, 5922-5929.
- 99 Z. Bian, T.Tachikawa, S.C.Cui, M.Fujitsuka, T. Majima, *Chem. Sci.*, 2012, **3**, 370-379.
- 100 E.A. Gibson, A.L. Smeigh, L. Le Pleux, L.Hammarström, F. Odobel, G. Boschloo, A. Hagfeldt, *J. Phys. Chem. C*, 2011, **115**, 9772-9779.
- 101 M.E. Orazem, B. Tribollet, *Electrochemical Impedance Spectroscopy*; John Wiley & Sons: Hoboken, NJ, 2008.
- 102 R. Kern, R. Sastrawan, J. Ferber, R. Stangl, J. Luther, *Electrochim. Acta*, 2002, **47**, 4213-4225.
- 103 Q. Wang, J.E. Moser, M. Gratzel, *J. Phys. Chem. B*, 2005, **109**, 14945-14953.
- 104 Z. Huang, G. Natu, Z. Ji, M. He, M. Yu, Y. Wu, *J. Phys. Chem. C*, 2012, **116**, 26239-26246.
- 105 X. L. Zhang, Z.P. Zhang, F.Z. Huang, P. Bauerle, U. Bach, Y.B. Cheng, *J. Mater. Chem.*, 2012, **22**, 7005-7009.
- 106 U. Bach et al. *Adv. En. Mater.*, 2014, **5**, 1401387.
- 107 I. Hod, Z. Tachan, M. Shalom, A. Zaban, *Phys.Chem. Chem. Phys.*, 2013, **15**, 6339-6343.

- 108 Q. Liu, L. Wei, S. Yuan, X. Ren, Y. Zhao, Z. Wang, D. Li, *Journal of Materials Science*, 2015, **50**, 6668–6676.
- 109 G. Natu, P. Hasin, Z. Huang, Z. Ji, M. Fe, Y. Wu, *ACS Appl. Mater. Interfaces*, 2012, **4**, 5922–5929.
- 110 G. Natu, Z. Huang, Z. Ji, Y. Wu, *Langmuir*, 2011, **28**, 950–956.
- 111 Y. Yu, X. Li, Z. Shen, X. Zhang, P. Liu, Y. Gao, J. Hua, *Journal of Colloid and Interface Science*, 2017, **490**, 380–390.
- 112 O. Langmar, D. Saccone, A. Amat, S. Fantacci, G. Viscardi, C. Barolo, D.M. Guldi, *ChemSusChem*, 2017, **10**, 2385–2393.
- 113 F. Odobel et al. *Adv. En. Mater.*, 2017, **7**, 1601776.
- 114 D.M. Guildi et al. *Nanoscale*, 2016, **8**, 17963–17975.
- 115 S. Sheehan, G. Naponiello, F. Odobel, D. P. Dowling, A. Di Carlo, D. Dini, *Journal of Solid State Electrochemistry*, 2014, **19**, 975–986.
- 116 L. D’Amario, G. Boschloo, A. Hagfeldt, L. Hammarström, *J. Phys. Chem. C*, 2014, **118**, 19556–19564.
- 117 L. Zhang, G. Boschloo, L. Hammarström and H. Tian, *Phys. Chem. Chem. Phys.*, 2016, **18**, 5080–5085.
- 118 T. T. Pham, S. K. Saha, D. Provost, Y. Farré, M. Raissi, Y. Pellegrin, E. Blart, S. Vedraïne, B. Ratier, D. Aldakov, F. Odobel and J. Bouclé, *J. Phys. Chem. C*, 2017, **121**, 129–139.
- 119 L. Favereau, J. Warnan, Y. Pellegrin, E. Blart, M. Boujtita, D. Jacquemin and F. Odobel, *Chem. Commun.*, 2013, **49**, 8018–8020.
- 120 U. Bach et al. *Electrochimica Acta*, **182**, 2015, 458–463.
- 121 S. Powar, D. Xiong, T. Daeneke, M.T. Ma, A. Gupta, G. Lee, S. Makuta, Y. Tachibana, W. Chen, L. Spiccia, *J. Phys. Chem. C*, 2014, **118**, 16375–16379.
- 122 E. L. Miller, R. E. Rocheleau, *J. Electrochem. Soc.*, 1997, **144**, 1995–2003.
- 123 C. J. Wood, G. H. Summers, C. A. Clark, N. Kaeffer, M. Bräutigam, L. R. Carbone, L. D’Amario, K. Fan, Y. Farré, S. Narbey, F. Oswald, L. A. Stevens, C. D. J. Parmenter, M. W. Fay, A. La Torre, C. E. Snape, B. Dietzek, D. Dini, L. Hammarström, Y. Pellegrin, F. Odobel, L. Sun, V. Artero and E. A. Gibson, *Phys. Chem. Chem. Phys.*, 2016, **18**, 10727–10738.
- 124 D. Dini, Y. Halpin, J. G. Vos, E. A. Gibson, *Coord. Chem. Rev.*, 2015, **304**, 179–201.
- 125 S. Sumikura, S. Mori, S. Shimizu, H. Usami and E. Suzuki, *J. Photochem. Photobiol. A: Chem.*, 2008, **199**, 1–7.
- 126 M. Awais, E. Gibson, J. G. Vos, D. P. Dowling, A. Hagfeldt and D. Dini, *ChemElectroChem*, 2014, **1**, 384–391.
- 127 Q. Wu, Y. Shen, L. Li, M. Cao, F. Gu and L. Wang, *Appl. Surf. Sci.*, 2013, **276**, 411–416.
- 128 S. Mori, S. Fukuda, S. Sumikura, Y. Takeda, Y. Tamaki, E. Suzuki and T. Abe, *J. Phys. Chem. C*, 2008, **112**, 16134–16139.
- 129 A. L. Smeigh, L. Le Pleux, J. Fortage, Y. Pellegrin, E. Blart, F. Odobel and L. Hammarstrom, *Chem. Commun.*, 2012, **48**, 678–680.
- 130 L. D’Amario, J. Fohlinger, G. Boschloo and L. Hammarstrom, *Chem. Sci.*, 2018, **9**, 223–230.
- 131 C. Xin, Y. Wang, S. Zhang, L. Xu, Y. Yu, H. Xiang, W. Wu, J. Hua, *Rapid research letter*, 2017, **11**, 1700258.
- 132 P. Ho, L. Q. Bao, K. S. Ahn, R. Cheruku and J. H. Kim, *Synthetic Met.*, 2016, **217**, 314–321.
- 133 W. Chen et al. *RSC Adv.*, 2014, **4**, 60670–60674.
- 134 E.A. Gibson et al. *ACS Appl. Mater. Interfaces*, 2015, **7**, 24556–24565.
- 135 X. Li et al. *Ceramics International*, 2016, **42**, 14565–14572
- 136 T. Ueda et al., *ChemElectroChem*, 2018, **5**, 823–838.
- 137 Y. V. Geletii, B. Botar, P. Kçgerler, D. A. Hillesheim, D. G. Musaev and C. L. Hill, *Angew. Chem. Int. Ed.*, 2008, **47**, 3896–3899.
- 138 H. D. Pratt III and T. M. Anderson, *Dalton Trans.*, 2013, **42**, 15650–15655.
- 139 J. J. Chen, M. D. Symes, S. C. Fan, M. S. Zheng, H. N. Miras, Q. F. Dong and L. Cronin, *Adv. Mater.*, 2015, **27**, 4649–4654.
- 140 P. Gómez-Romero, M. Chojak, K. Cuentas-Gallegos, J. A. Asensio, P. J. Kulesza, N. Casañ-Pastor and M. Lira-Cantffl, *Electrochem. Commun.*, 2003, **5**, 149–153.
- 141 H. El Moll, F. A. Black, C. J. Wood, A. Al-Yasari, M. Reddy Marri, I. V. Sazanovich, E. A. Gibson and J. Fielden, *Phys. Chem. Chem. Phys.*, 2017, **19**, 18831–18335.
- 142 J.N.H Reek et al. *Sustainable Energy Fuels*, 2019, **3**, 96–100.
- 143 C.A Bignozzi et al *Chem. Eur. J.* 2010, **16**, 2611 – 2618.
- 144 K.O Ukoba et al. *Renewable and Sustainable Energy Reviews*, 2018, **82**, 2900–2915.
- 145 T.S. Natarajan et al. *J. Mater. Chem. A*, 2015, **3**, 7513–7522.
- 146 B. Jousselve et al. *ACS Appl. Mater. Interfaces*, 2017, **93**, 2369–2677.
- 147 E.A. Gibson et al. *Phys. Chem. Chem. Phys.*, 2016, **18**, 10727–10738
- 148 H. B. Yang, G. H. Guai, C. X. Guo, Q. L. Song, S. P. Jiang, Y. L. Wang, W. Zhang and C. M. Li, *J. Phys. Chem. C*, 2011, **115**, 12209–12215.
- 149 S. Sumikura, S. Mori, S. Shimizu, H. Usami, E.Suzuki *J. Photochem. Photob. A* , 2008, **194**, 143–147.
- 150 O. Langmar, C. R. Ganivet, A. Lennert, R. D. Costa, G. de la Torre, T. Torres, D. M. Guldi, *Angew. Chem. Int. Ed.*, 2015, **54**, 7688–7692.
- 151 D.M. Guildi et al. *ACS Appl. Energy Mater.*, 2018, **1**, 6388–6400.
- 152 D.M Guildi et al. *J. Mater. Chem. C*, 2018, **6**, 5176–5180.
- 153 O. Langmar, E. Fazio, G. De la Torre, T. Torres, R. Costa, D.M. Guldi, *Angew. Chem. Int. Ed.*, 2018, **131**, 4097–4102.
- 154 F. Odobel et al. *RSC Adv.*, 2016, **6**, 112765–112770.
- 155 L. Dou, F. Cui, Y. Yu, G. Khanarian, S.W. Eaton, Q. Yang, J. Resasco, C. Schildknecht, K. Schierle-Arndt, P. Yang, *ACS Nano*, **10**, 2600–2606.
- 156 S. Du, P. Cheng, P. Sun, B. Wang, Y. Cai, F. Liu, J. Zheng, G. Lu, *Chemical Research in Chinese Universities*, 2014, **30**, 661–665.
- 157 S. Jobic et al. *Journal of Alloys and Compounds*, 2018, **769**, 605–610.
- 158 M.K. Gumpta et al. *J. Appl. Phys.*, 2011, **109**, 083532.
- 159 J. Bai, X. B. Xu, L. Xu, J. Cui, D. K. Huang, W. Chen, Y. B. Cheng, Y. Shen and M. K. Wang, *ChemSusChem*, 2013, **6**, 622–629.
- 160 L. Schmidt-Mende, J. MacManus-Driscoll, *Mater. Today*, 2007, **10**, 40 – 48
- 161 Z. Huang, M. He, M. Yu, K. Click, K., D. Beauchamp, Y. Wu, *Angew. Chem. Int. Ed.*, 2015, **54**, 6857–6861.
- 162 Z. Yu, I. R. Perera, T. Daeneke, S. Makuta, Y. Tachibana, J. J. Jasieniak, A. Mishra, P. Bauerle, L. Spiccia and U. Bach, *NPG Asia Mater*, 2016, **8**, e305.
- 163 H. Hosono et al. *Nature*, 1997, **389**, 939–942.
- 164 W. Watson et al. *J. Chem. Phys.*, 2010, **132**, 024707.
- 165 J. Bandara and J. P. Yasomanee, *Semicond. Sci. Tech.*, 2007, **22**, 20–24.
- 166 A. Nattestad, X. L. Zhang, U. Bach and Y. B. Cheng, *J. Photon. Energy*, 2011, **1**, , 011103.
- 167 J. Ahmed, C. K. Blakely, J. Prakash, S. R. Bruno, M. Z. Yu, Y. Y. Wu and V. V. Poltavets, *J. Alloy Compd.*, 2014, **591**, 275–279.
- 168 M. Miclau, N. Miclau, R. Banica and D. Ursu, *Mater. Today-Proc.*, 2017, **4**, 6975–6981.
- 169 M. Z. Yu, G. Natu, Z. Q. Ji and Y. Y. Wu, *J. Phys. Chem. Lett.*, 2012, **3**, 1074–1078.
- 170 A. Renaud, L. Cario, P. Deniard, E. Gautron, X. Rocquefelte, Y. Pellegrin, E. Blart, F. Odobel and S. Jobic, *J. Phys. Chem. C*, 2014, **118**, 54–59.
- 171 D. Ursu, M. Miclau, R. Banica and N. Vaszilcsin, *Mater. Lett.*, 2015, **143**, 91–93.

- 172 Z. Xu, D. H. Xiong, H. Wang, W. J. Zhang, X. W. Zeng, L. Q. Ming, W. Chen, X. B. Xu, J. Cui, M. K. Wang, S. Powar, U. Bach and Y. B. Cheng, *J. Mater. Chem. A*, 2014, **2**, 2968-2976.
- 173 D. Ursu et al. *J. Mater. Eng. Perform.*, 2016, **25**, 59-63.
- 174 D.O. Scanlon et al. *J. Chem. Phys.* 2010, **132**, 024707.
- 175 D.O. Scanlon et al. *J. Mater. Chem.*, 2011, **21**, 3655.
- 176 Y-B.Cheng et al. *J. Mater. Chem.*, 2012, **22**, 24760-24768.
- 177 U. Bach et al. *J. Phys. Chem. C*, 2014, **118**, 16375-16379
- 178 S.Mori, S.Fukuda, S.Sumikura, Y. Takeda, Y. Tamaki, E. Suzuki, T.Abe, T., *J. Phys. Chem. C*, 2008, **112**, 16134-16139.
- 179 W.Chen et al. *Scientific Reports*, 2014, **4**, 3961.
- 180 W.Chen et al. *ChemSusChem*. 2013, **6**, 1432-1437.
- 181 M. Miclau et al. *Energy Procedia* 2017, **112**, 497-503.
- 182 W. Chen et al. *Journal of Alloys and Compounds*, 2016, **662**, 374-380.
- 183 M.A. Marquardt, N.A. Ashmore, D.P. Cann, *Thin Solid Films*, 2006, **496**, 146-156.
- 184 D.H. Choi, S.J. Moon, J.S. Hong, S.Y. An, I.-B. Shim, C.S. Kim, *Thin Solid Films*, 2009, **517**, 3987-3989.
- 185 A. Barnabé, E. Mugnier, L. Presmanes, P. Tailhades, *Mater. Lett.*, 2006, **60**, 3468-3470.
- 186 E. Mugnier, A. Barnabé, L. Presmanes, P. Tailhades, *Thin Solid Films*, 2008, **516**, 1453-1456.
- 187 H. Y. Chen and J. H. Wu, *Thin Solid Films*, 2012, **520**, 5029-5035.
- 188 T. Kajitani et al. *Japanese Journal of Applied Physics*, 2007, **46**, 8A .
- 189 Z. Deng et al. *Journal of Alloys and Compounds*, 2013, **577**, 658-662.
- 190 T. Zhu, Z. H. Deng, X. D. Fang, Z. P. Huo, S. M. Wang, W. W. Dong, J. Z. Shao, R. H. Tao, C. Song and L. Wang, *Journal of Alloys and Compounds*, 2016, **685**, 836-840.
- 191 T. F. Jiang, M. Bujoli-Doeuff, Y. Farre, E. Blart, Y. Pellegrin, E. Gautron, M. Boujtita, L. Cario, F. Odobel and S. Jobic, *RSC Adv.*, 2016, **6**, 1549-1553.
- 192 H. Hosono *Thin Solid Films*, 2007, **515**, 6000-6014.
- 193 K. Ueda, S.Inoue, S.Hirose, H.Kawazoe, H. Hosono, *Appl. Phys. Lett.*, 2000, **77**, 2701-2703.
- 194 H. Hiramatsu, et al. *Appl. Phys. Lett.*, 2003, **82**, 1048-1050.
- 195 A. Renaud, L. Cario, Y. Pellegrin, E. Blart, M. Boujtita, F. Odobel and S. Jobic, *RSC Adv.*, 2015, **5**, 60148-60151.
- 196 T. Y. Wei, C. H. Chen, H. C. Chien, S. Y. Lu, C. C. Hu, *Adv. Mater.* 2010, **22**, 347-351.
- 197 T.W. Hamann, *Dalton Trans.*, 2012, **41**, 3111-3115.
- 198 F.A. Benko et al. *J. Appl. Phys.*, 1982, **53**, 1173.
- 199 P. Patil, L. Kadam, *Applied surface science*, 2002, **199**, 211-221.
- 200 M.D. Irwin, D.B. Buchholz, A.W. Hains, R.P. Chang, T.J. Marks, *Academy of Sciences*, 2008, **105**, 2783-2787.
- 201 S. Das, S. Saha, D. Sen, U.K. Ghorai, D. Banerjee, K.K. Chattopadhyay, *J. Mater. Chem. C*, 2014, **2**, 1321-1330.
- 202 A. Renaud, B. Chavillon, L. Le Pleux, Y. Pellegrin, E. Blart, M. Boujtita, T. Pauporte, L. Cario, S. Jobic, F. Odobel, F., *J. Mater. Chem.*, 2012, **22**, 14353-14356.
- 203 D. Dini, Y. Halpin, J.G. Vos, E.A. Gibson, E. A., *Coord. Chem. Rev.*, 2015, **304**, 179-201.
- 204 W. Spear, D. Tannhauser, *Physical Review B*, 1973, **7**, 831.
- 205 Y. Duan, X. Liu, L. Han, S. Asahina, D. Xu, Y. Cao, Y. Yao, S. Che, *J. Am. Chem. Soc.*, 2014, **136**, 7193-7196.
- 206 D.S. Murali, S. Kumar, R. Choudhary, A.D. Wadikar, M.K. Jain, A. Subrahmanyam, *AIP Adv.*, 2015, **5**, 047143.
- 207 J. Yu, S. Zhuang, X. Xu, W. Zhu, B. Feng, J. Hu, *J. Mater. Chem. A*, 2015, **3**, 1199-1207.
- 208 Y.K. Hsu, C.H. Yu, CY.C. Chen, Y.G. Lin, *Electrochimica Acta* 2013, **105**, 62-68.
- 209 P.A. Korzhavyi, B. Johansson, *Swedish Nuclear Fuel and Waste Management Co.*: 2011.
- 210 R. Srinivasan, B. Chavillon, C. Doussier-Brochard, L. Cario, M. Paris, E. Gautron, P. Deniard, F. Odobel, S. Jobic, *J. Mater. Chem.*, 2008, **18**, 5647-5653.
- 211 K. Ueda, T. Hase, H. Yanagi, H. Kawazoe, H. Hosono, H. Ohta, M. Orita, M. Hirano, *J. Appl. Phys.*, 2001, **89**, 1790-1793.
- 212 R. Gillen, J. Robertson, *Physical Review B*, 2011, **84**, 035125.
- 213 M. Lee, D. Kim, Y. T. Yoon, Y. I. Kim, *Bull. Korean Chem. Soc*, 2014, **35**, 3261-3266.
- 214 T. Ahmad, R. Phul, P. Alam, I.H. Lone, M. Shahazad, J. Ahmed, T. Ahamad, S.M. Alshehri, *RSC Adv.*, 2017, **7**, 27549-27557.
- 215 W. Ketir, S. Saadi, M. Trari, *Journal of Solid State Electrochemistry*, 2012, **16**, 213-218.
- 216 M. Soda, K. Kimura, T. Kimura, K. Hirota, *Physical Review B*, 2010, **81**, 100406.
- 217 R.S. Yu, C.M. Wu. *Applied Surface Science*, 2013, **282**, 92-97.
- 218 A. Ioakeimidis, I.T. Papadas, D. Tsikritzis, G.S. Armatas, S. Kennou, S.A. Choulis, *APL Materials*, 2019, **7**, 021101.
- 219 B. Cui, H. Lin, Y.Z. Liu, J.B. Li, P. Sun, X.C. Zhao, C.J. Liu, *J. Phys. Chem. C*, 2009, **113**, 14083-14087
- 220 Y. Wan, J. Chen, J. Zhan, Y. Ma, *Journal of environmental chemical engineering*, 2018, **6**, 6079-6087.
- 221 H. Yanagi, S.I. Inoue, K. Ueda, H. Kawazoe, H. Hosono, N. Hamada, *J. Appl. Phys.*, 2000, **88**, 4159-4163.
- 222 F. Benko, F. Koffyberg, *Journal of Physics and Chemistry of Solids*, 1984, **45**, 57-59.
- 223 B. Das, A. Renaud, A.M. Volosin, L. Yu, N. Newman, D.K. Seo, *Inorganic chemistry*, 2015, **54**, 1100-1108.
- 224 B.J. Ingram, T.O. Mason, R. Asahi, K. Park, A. Freeman, *Physical Review B*, 2001, **64**, 155114.
- 225 H. Kawazoe, M. Yasukawa, H. Hyodo, M. Kurita, H. Yanagi, H. Hosono, *Nature*, 1997, **389**, 939-942.
- 226 H.Y. Chen, J.H. Wu, *Applied Surface Science*, 2012, **258**, 4844-4847.
- 227 M.S. Prévot, X.A. Jeanbourquin, W.S. Bourée, F. Abdi, D. Friedrich, R. Van De Krol, N.S. Guijarro, F. Le Formal, K. Sivula, *Chemistry of Materials*, 2017, **29**, 4952-4962.
- 228 H.Y. Chen, J.H. Wu, *Thin Solid Films*, 2012, **520**, 5029-5035.
- 229 S. Santra, N.S. Das, D. Sen, K.K. Chattopadhyay, *J. Phys. D: Appl. Phys.*, 2014, **47**, 505301.
- 230 M.S. Miao, S. Yarbro, P.T. Barton, R. Seshadri, *Physical Review B*, 2014, **89**, 045306.
- 231 K. Ueda, S. Inoue, H. Hosono, N. Sarukura, M. Hirano, *Appl. Phys. Lett.*, 2001, **78**, 2333-2335.
- 232 K. Ueda, S. Inoue, S. Hirose, H. Kawazoe, H. Hosono, *Appl. Phys. Lett.*, 2000, **77**, 2701-2703.
- 233 K. Ueda, H. Hosono, *J. Appl. Phys.*, 2002, **91**, 4768-4770.
- 234 A. Renaud, L. Cario, Y. Pellegrin, E. Blart, M. Boujtita, F. Odobel, S. Jobic, *RSC Adv.*, 2015, **5**, 60148-60151.
- 235 K. Aiempanakit, P. Rakkwamsuk, S. Dumrongrattana, J. Kasetsart. *Nat. Sci.*, 2008, **42**, 351-356.
- 236 T.S. Tripathi, M. Karppinen, *Adv. Mater. Inter.*, 2017, **4**, 1700300.
- 237 Z. Yu, I.R. Perera, T. Daeneke, S. Makuta, Y. Tachibana, I.J. Jasieniak, A. Mishra, P. Bäuerle, L. Spiccia, U. Bach, *NPG Asia Materials*, 2016, **8**, e305.
- 238 M.S. Lee, I.C. Cheon, Y.I. Kim, *Bulletin of the Korean Chemical Society* 2003, **24**, 1155-1162.
- 239 T.A. König, P.A. Ledin, J. Kerszulis, M.A. Mahmoud, M.A. El-Sayed, J.R. Reynolds, V.V. Tsukruk, *ACS nano*, 2014, **8**, 6182-6192.
- 240 H. Haitjema, J.P. Elich, *Thin solid films*, 1991, **205**, 93-100.
- 241 J. Ederth, P. Heszler, A. Hultåker, G. Niklasson, C. Granqvist, *Thin solid films*, 2003, **445**, 199-206.